InSAR measured permafrost degradation of palsa peatlands in northern Sweden

Authors: Samuel Valman[1,2]*, Matthias B. Siewert[3]*, Doreen Boyd[2], Martha Ledger[4,5], David Gee[6], Betsabe de la Barreda-Bautista[4,2], Andrew Sowter[6], Sofie Sjogersten[4]

Affiliations:

[1] Nottingham Geospatial Institute, University of Nottingham, Nottingham NG7 2TU, UK

[2] School of Geography, University of Nottingham, University Park, NG7 2RD, Nottingham, UK

[3] Department of Ecology and Environmental Sciences, Umeå University, Umeå, Sweden

[4] School of Biosciences, University of Nottingham, Sutton Bonington Campus, College Road, LE12 5RD, Loughborough, UK

[5] School of Biological Sciences, Kadoorie Biological Sciences Building, University of Hong Kong, Pok Fu Lam Road, Hong Kong

[6] TerraMotion, Ingenuity Centre, Triumph Rd, Nottingham NG7 2TU

*These authors contributed equally to this work.

Corresponding author: Sofie Sjögersten sofie.sjogersten@nottingham.ac.uk

Abstract. Climate warming is degrading palsa peatlands across the circumpolar permafrost region. Permafrost degradation may lead to ecosystem collapse and potentially strong climate feedbacks, as this ecosystem is an important carbon store and can transition to being a strong methane emitter. Landscape level measurement of permafrost degradation is needed to monitor this impact of warming. Surface subsidence is a useful metric of change and can be monitored using InSAR satellite technology. We combined InSAR data, processed using the ASPIS algorithm to monitor ground motion between 2017 and 2021, with airborne optical and LiDAR data to investigate the rate of subsidence across palsa peatlands in northern Sweden. We show that 55% of the area of Sweden's eight largest palsa peatlands areis currently subsiding, which can be attributed to these permafrost landforms and their degradation. The most rapid degradation occurring in the largest palsa complexes in the most northern part of the region of study, also corresponding to the areas with the highest % palsa cover within the overall mapped wetland area. Further, higher degradation rates were found in areas where winter precipitation has increased substantially. The roughness index calculated from a LiDAR-derived DEM, used as a proxy for degradation, increases alongside subsidence rates and may be used as a complementary proxy for palsa degradation. We show that combining datasets captured using remote sensing enables regional-scale estimation of ongoing permafrost degradation, an important step to–wards estimating the future impact of climate change on permafrost-dependent ecosystems.

Keywords: Permafrost, subsidence, Arctic, InSAR, palsa, peatlands

36

~~2.0~~**1.0** **Introduction**

38 Permafrost regions are critical components in the climate system, due to their essential carbon (C) storage
39 service (Harris et al., 2022). The circumpolar permafrost region in particular, stores around 1300±200 Pg of
40 organic C, corresponding to around 50% of the global terrestrial C pool (Hugelius et al., 2020; Köchy et al.,
41 2015). It covers around 21 million km^2 or 22% of the Northern Hemisphere's ~~landscapes~~ exposed land surface
42 (Obu, 2021). Northern peatlands themselves store an estimated 415±150 Pg of C in an area covering around 3.7
43 million km^2 of which around 1.7 million km^2 is permafrost ~~substantially within~~overlapping with the circumpolar
44 permafrost region in discontinuous and sporadic permafrost zones (Hugelius et al., 2020). Permafrost in these
45 peatlands raises the surface above the water table forming so-called palsa (pl. palsas) or, in extended form, peat
46 plateau~~x~~s (Seppälä, 2011). These account for substantial areas of global permafrost, including in northern
47 Fennoscandia (Ballantyne ~~C. K.~~, 2018; Gisnås et al., 2017; Tarnocai et al., 2009)~~;~~. ~~for example, i~~In northern
48 Sweden, 137 km^2 of th~~ese~~is palsa ~~peatland has~~have been recorded from field reports~~reported~~ (Backe, 2014).
49 Climate warming, and the associated alteration in the precipitation regime, is increasingly recognized to be a
50 particular threat to permafrost (Biskaborn et al., 2019), with the subarctic Fennoscandian permafrost region, and
51 the palsa ~~peatlands~~ within, particularly vulnerable (Christiansen et al., 2010; Farbrot et al., 2013).

52 Climatic models project unsuitable conditions for permafrost within the coming century, with the most pessimistic
53 estimates projecting unsuitability even sooner - by 2040 in Fennoscandia (Chadburn et al., 2017; Fewster et al.,
54 2022; Könönen et al., 2022; Stefan et al., 2006). As palsa ~~peatlands~~ are often found in the sporadic or
55 discontinuous permafrost zone (Zuidhoff & Kolstrup, 2000), they are particularly sensitive to climate warming
56 and any resultant permafrost thaw and disappearance. Their sensitivity mainly results from the alterations in the
57 thermal insulation effect of peat deposits and snow as the climate changes (Seppälä, 2011; Smith & Riseborough,
58 1996). Specifically, organic peat has a high thermal conductivity when wet and frozen, but low conductivity when
59 dry and thawed. Snow has a highly insulating effect on ground temperature. Thus, extended periods of air-
60 temperatures below 0°C and thin snow cover in winter are beneficial to maintain or grow the perennial frozen
61 ~~permafrost~~ core of palsas and peat plateau~~x~~s. Low summer precipitation, which reduces the thermal conductivity
62 of peat, also helps to preserve the frozen cores in palsa. In contrast, increased snowfall has been linked to
63 permafrost degradation as it increases winter insulation. Further, high summer precipitation leads to higher
64 thermal conductivity of peat, and combined with warm summer temperatures, can degrade permafrost by
65 increasing permafrost temperatures and subsequent thawing of the frozen peat core of palsas. The strong insulating
66 properties of peat allow the occurrence of permafrost at the southern extent of the northern permafrost region and
67 valley bottoms in areas otherwise too warm for permafrost (Johansson et al., 2013; Seppälä, 2011; Smith &
68 Riseborough, 1996).

69 Warming of the permafrost in palsa ~~peatlands~~ typically leads at the surface, to top-down thaw, (i.e. thickening of
70 the active layer), and eventual subsidence of the surface, as well as lateral thaw, sometimes called abrupt thaw
71 or thermokarst, which occurs at the margin of peat plateaux and palsa edges (Seppälä, 2011; Smith &
72 Riseborough, 1996; Zuidhoff, 2002). This is often associated with water-logged conditions and, as a result,
73 increased methane (CH$_4$) emissions (Glagolev et al., 2011; Hugelius et al., 2020; Matthews et al., 1997;
74 Miglovets et al., 2021; Schuur et al., 2009; Turetsky et al., 2020; Varner et al., 2022), which is a central theme
75 for permafrost research (Sjöberg *et al.*, 2020). A subsequent impact of this permafrost degradation is an
76 alteration in vegetation cover, its hydrology, and human use of the landscape (e.g., infrastructure and reindeer
77 husbandry)(Markkula et al., 2019; Ramage et al., 2021). Given the potentially large impacts of permafrost thaw
78 on the global climate, ecosystem function and human activity, quantification and monitoring of the subsidence
79 in peat deposits affected by permafrost thaw and degradation, as well as an understanding of their sensitivity to
80 changing climatic parameters, is urgently required (IPCC, 2021).

81 The degradation of the permafrost of palsa~~s~~ ~~peatlands~~ has been observed right across the circumpolar
82 permafrost region in a number of studies, including in northern Scandinavia (Åkerman & Johansson, 2008; de la
83 Barreda-Bautista et al., 2022; Luoto & Seppälä, 2003; Olvmo et al., 2020; Sannel et al., 2016; Varner et al.,

84   2022); Russia (Glagolev et al., 2011; Miglovets et al., 2021; van Huissteden et al., 2021); the USA (Douglas et
85   al., 2021; Douglas et al., 2015; Sannel, 2020) and Canada (Mamet et al., 2017; Sannel & Kuhry, 2011; Short et
86   al., 2014; Vallée & Payette, 2007). Although rapid degradation in response to short term climatic events has
87   been observed, typically permafrost degradation has been investigated via long-term monitoring at decadal
88   timescales in response to changes in temperature and precipitation conditions (Åkerman & Johansson, 2008; de
89   la Barreda-Bautista et al., 2022; Olvmo et al., 2020; Sannel et al., 2016). These longer-term studies have shown
90   strong relationships between permafrost degradation and summer temperatures, length of the thaw period,
91   winter precipitation and snow depth (Smith et al., 2022). These types of analyses are very useful for quantifying
92   how much of the landscape has already transitioned and understanding the climate change drivers behind these
93   changes, but they do not capture the initial stages of permafrost degradation in palsas ~~peatlands~~ and the lower
94   rates of subsidence that have yet to result in observable changes in the vegetation or thermokarst formation. The
95   latter is crucial to understand the ongoing response of palsas ~~peatlands~~ to climate warming and to predict when
96   pulses of greenhouse gases to the atmosphere and other impacts (e.g., on infrastructure) are likely to occur.
97   Thus, we need approaches that detect early signs of degradation at landscape scales, with repeated observations. ~~,~~
98   ~~are urgently required.~~

99   Due to the vast extent and remoteness of permafrost areas there is no current complete annual degradation rate
100   measurements. So, ~~,~~ we looked to satellite remote sensing to underpin the measurement and monitoring
101   assessment of permafrost peatlands, their degradation and resultant climate impacts (~~Armstrong McKay et al.,~~
102   ~~2022;~~ Hugelius et al., 2020~~; Obu, 2021~~; ~~Schuur et al., 2015;~~ Swingedouw et al., 2020). Optical remote sensing
103   approaches can be augmented with RaDAR remote sensing methods, including InSAR, to capture the early
104   response of permafrost to warming. ~~, since T~~these methods can detect vertical land surface motion at millimetre
105   precision across a range of natural landscapes, with greater confidence in the direction of surface motion than
106   the absolute magnitude (Alshammari et al., 2020; Alshammari et al., 2018; Bartsch *et al.*, 2016; de la Barreda-
107   Bautista et al., 2022; Short et al., 2014; van Huissteden et al., 2021) ~~(Bartsch *et al.*, 2016)~~. The regular sampling
108   frequency, insensitivity to cloud and, in the case of Sentinel-1, low cost, means InSAR from Sentinel-1 should
109   be well suited to measure and monitor ongoing changes in permafrost affected by climate change. Further,
110   Sentinel-1 for InSAR is effective at both local and regional scales - the 20m × 20m spatial resolution enables
111   measurement of surface motion within local sites (de la Barreda-Bautista et al., 2022), and can do so over entire
112   and complex landscapes, such as the circumpolar permafrost region (Reinosch et al., 2020).

113   The overall aim of this study was to carry out a regional-scale analysis of permafrost degradation across the
114   palsas ~~peatlands~~ of northern Sweden, principally using Sentinel-1 InSAR-derived subsidence as an indication of
115   degradation. Pertinent to this is that any InSAR-detected changes can be associated with known and delineated
116   targets in the wider landscape. Furthermore, it is also important to understand any within-site dynamics of
117   permafrost degradation. This paper therefore has specific objectives to: (i) measure the subsidence rate between
118   2017-2021 of all major palsa ~~peatlands~~ complexes in the northern Sweden region; (ii) determine in which palsa
119   ~~peatlands~~ complexes subsidence is greatest, and (iii) assess if the spatial patterns of degradation can be linked to
120   climatic variables and properties of the different sites across the region. To achieve these objectives, we
121   combined large-scale regional analysis with higher resolution site-specific analysis of patterns in subsidence,
122   using a combination of datasets - satellite (Sentinel-1) InSAR; occupied airborne optical and LiDAR data; and
123   snow depth, precipitation, and temperature time-series from meteorological stations across the region.

124

2.0 Methodology

2.1 Study area

This study focused on the northern part of Sweden; a region containing palsa peatlands, located between 68.84-67.64° N and 18.71-21.19° E. The palsas peatlands of the region are confined predominantly to valley bottoms in an elevation range between ca. 350 and 590m asl (Fig. 1). The rest of the study area region is comprised of forests and/or mountain land covers (Siewert, 2018; Åkerman & Johansson, 2008). Of all the palsas in the region, the eight largest palsa peatlands complexes of concentrated palsa range between 50 and 273ha in area (Table 1). These were located across the region, which covers a ca. 20,000km² area, with the largest palsa sites located in the north-western parts of the region. Smaller palsas peatlands occur scattered in distribution right across the region. The climate varies across the region from north to south (www.smhi.se). The mean January and July temperatures in Karesuando in the northern part of the study region is -16 and 12.8°C, respectively, while in Kiruna, slightly further south, the mean January January, and July temperatures is -11.6 and 13.4C (1991-2020 average). Mean annual precipitation is 443 and 560mm in Karesuando and Kiruna, respectively.

138

139
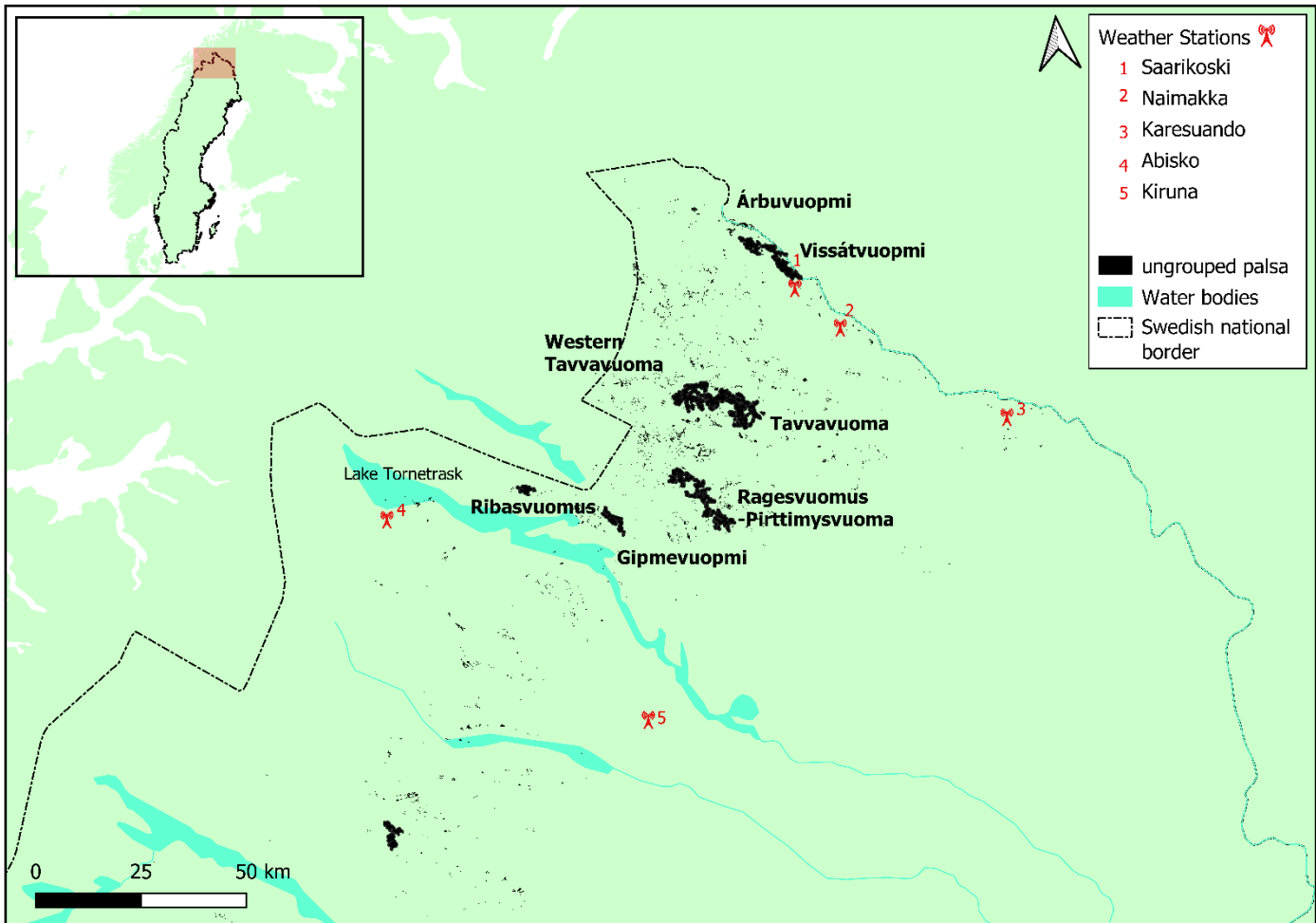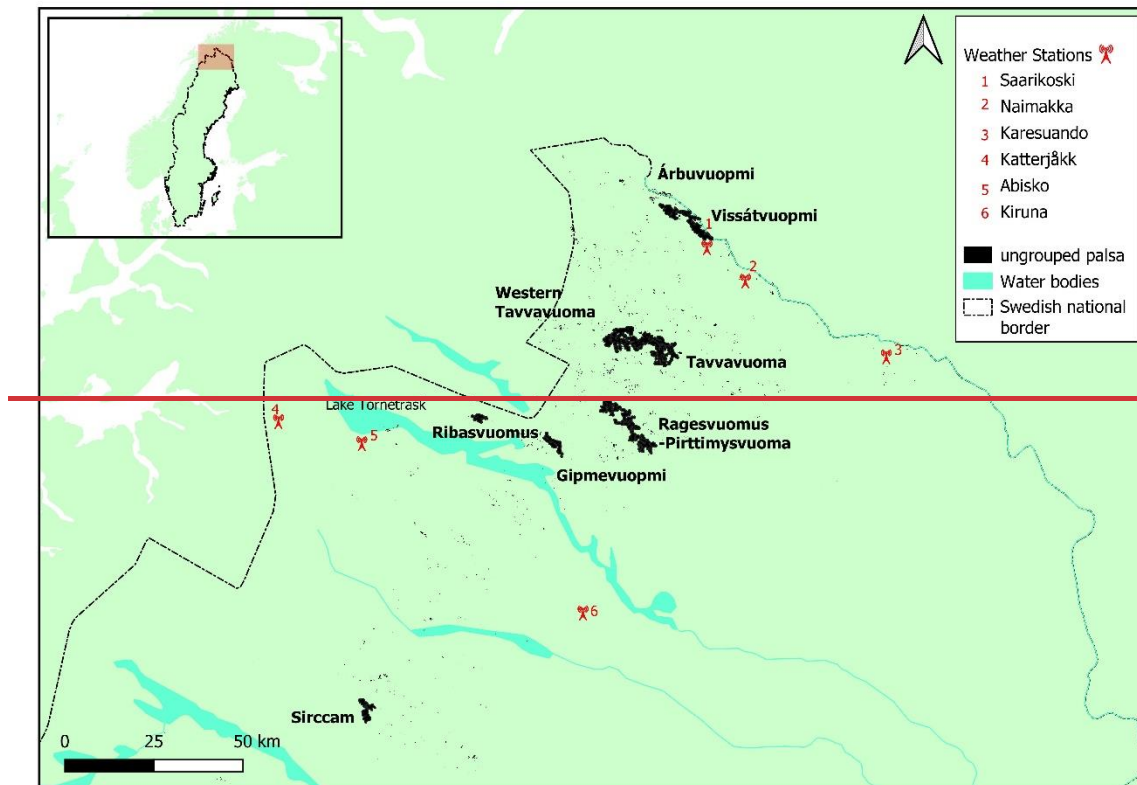
Figure. 1: Map of the palsa ~~peatland complexes~~ *in Sweden which were investigated in the study focusing on the eight named palsa* ~~peatlands~~*complexes.* *The black regions show all the palsa which has been reported to exist (Backe, 2014,) with the larger named areas displaying the 250m buffers around the palsa areas which have created continuous expanses.* ~~The black regions show where 250m buffers around the palsa areas have created continuous expanses (Backe, 2014).~~ *Meteorological station positions used in the study are also indicated.*

A previous national palsa mapping dataset provided raster cells at a spatial resolution of 100m, with the % palsa cover computed and a 250m buffered output to provide continuous palsa area outputs (Backe, 2014). This afforded analyses at a spatial resolution suitable for analysis with Sentinel-1 yet provide practical representation of the condition of the palsa in this region. All these data were analysed in this study, but the eight largest continuous areas of these palsa (Backe, 2014) were focused on, hereon in referred to as palsa complexes, a term reflecting their mosaic nature of raised palsa and/or peatland plateaux, interspersed with lower lying fen or thermokarst areas. These eight sites account for the majority of the palsa areas in Sweden, the sites are listed in Table 1 along with some associated information on their status and total and raised palsa plateaux areas.

~~We selected larger palsa areas of the region to focus our analysis. This was in line with focus areas by the mapping of palsas undertaken as part of a previous national palsa peatland mapping effort (Backe, 2014). The resultant palsa peatland mapping dataset has a spatial resolution of 100m, with the % palsa cover for each pixel computed, and these pixels given a 250m buffer to produce continuous area outputs. The eight largest continuous areas of these palsa peatlands from the national palsa mapping dataset were selected for this study (Backe, 2014), hereon in referred to as palsa complexes, a term reflecting their mosaic nature of raised palsa plateaux, interspersed with lower lying fen or thermokarst areas. This afforded analyses at a spatial resolution suitable for analysis with Sentinel 1 yet provide practical representation of the condition of the peatland in the region. These eight sites account for the majority of the palsa peatland areas in Sweden, the sites are listed in Table 1 along with some associated information on their status and total and raised palsa plateau areas.~~

5

166

Table. 1: Information on the major palsa complexes analysed in this paper (Backe, 2014). The protection status
means no or limited direct anthropogenic activities that may influence palsa degradation. Total site area is
calculated from the total number of 100m × 100m palsa pixels at each site - these pixels have associated
percentages for how much of the 100m x 100m area is palsa. The average of these percentages for each site
displays the palsa density at each site. These percentages are then used to calculate the "total palsa area" for
each site based on the original report estimates.

| Site Name	Protection Classification	Total site area (ha)	Average extent palsa in these areas (%)	Total palsa area (ha)	LiDAR Collection year	Central location (Latitude, Longitude)
Árbuvuopmi	Not protected	327	26.3	86.06	2018, 2016	21.03464, 68.83842
Vissátvuopmi	Not protected	867	31.6	273.75	2015, 2018	21.19497, 68.79412
Tavvavuoma	EU Naturae 2000 SPA, SAC. Site of National Importance for Nature conservation	1719	15.8	271.25	2018	20.85043, 68.51132
Western Tavvavuoma	EU Natura e 2000 SPA, SAC. Site of National Importance for Nature conservation	813	13.0	105.74	2018	20.57727, 68.53953
Gipmevuopmi	Pristine mountain forest, Nature reserve, EU Naturae 2000 SCI	303	23.0	69.62	2013	20.09767, 68.28377
Ragesvuomus-Pirttimysvuoma	Pristine mountain forest, Nature reserve, EU Naturae 2000 SCI	881	6.55	57.74	2013	20.48660, 68.3741
Sirccam	EU Naturae 2000 SCI	397	12.8	50.70	2015	18.71528, 67.64537
Ribasvuomus	Pristine mountain forest, Nature reserve, EU Natura e 2000 SCI	216	23.2	50.13	2014	19.60100, 68.36116

173

174

2.2 Datasets

The InSAR-derived dataset of surface motion over this northern Sweden region of study was calculated for the period between 2017 to 2021, from single look complex (SLC) C-band SAR data, captured in Interferometric Wide (IW) Swath mode by the Sentinel-1 constellation (European Union's Copernicus Programme; Torres et al., 2012). SAR data input were from the thaw season when there was minimal coverage of snow and ice (i.e., between April and October in each year). Data from descending tracks 168 and 66 were used to cover the target area. Four stacks were processed independently with one from track 168 and three from track 66, which was split into a northern, middle, and southern subsets. The APSIS (formerly ISBAS) method (Sowter et al., 2013; Sowter et al., 2016) was used to characterize surface motion which relaxes the need for consistent phase stability and therefore enables near-complete spatial and temporal coverage over vegetated surfaces (Alshammari et al., 2020; Alshammari et al., 2018; Bradley et al., 2022; Cigna & Sowter, 2017; Gee et al., 2017; Sowter et al., 2016), including those found across snow-free permafrost regions.

InSAR processing of Sentinel-1 IW SLC imagery involves a series of steps summarised in Figure 2. Firstly, deburst and merging involved combining individual sub-swaths into a single wide-area SLC product. Secondly, the process of deramping produced a product where the problem of an ambiguous and rapidly changing phase with azimuth was solved for; a specific deramping function is available for Sentinel-1 data (ESA, 2015). Next step involved the co-registration of each Sentinel-1 image to a common slant range coordinate system and multi-looking of data by factors of 5 m7 in range and 20 m by2 azimuth. This produced a dataset with an approximate spatial resolution of 20m × 20m. Using a perpendicular baseline of 250m and maximum temporal baseline of 183

days ~ 2100 interferograms were generated per stack. The temporal baseline was chosen to balance the need to reduce the baseline to minimise phase ambiguities and best maintain coherence across the region, whilst also using a baseline long enough to generate season-to-season pairs over consecutive years. This is required over permafrost regions to capture more subtle trends of surface motion during the thaw period (de la Barreda-Bautista et al., 2022; Liu et al., 2010). The interferograms were unwrapped using a modified version of the SNAPHU algorithm (Shen et al., 2002), which converts circular phase data into a linear measure of deformation. The algorithm was modified in order to allow the ability to parallelise and to spread the calculation across multiple cores (Chen and Zebker, 2002). by ... because ... The multi-annual average velocity was calculated for pixels which maintained a coherence greater than 0.45 in a minimum of ~ 650 interferograms, with respect to stable reference points located in the town Kautekenio (N°69.00, E°23.04) for track 168 and Narvik (N°68.44, E°17.42), Kvikkjokk (N°66.95, E°17.72), and Rognan (N°67.09) for the subsets of track 66. The line-of-sight measurements were converted to vertical surface displacement using a cosine correction and finally mosaicked into a single deformation product. Localised UAV studies at sites in Sweden have verified the accuracy ability to of uuseing InSAR as a tool to monitor permafrost degradation (de la Barreda-Bautista et al., 2022). We summarise the steps for InSAR data processing in Figure 2.
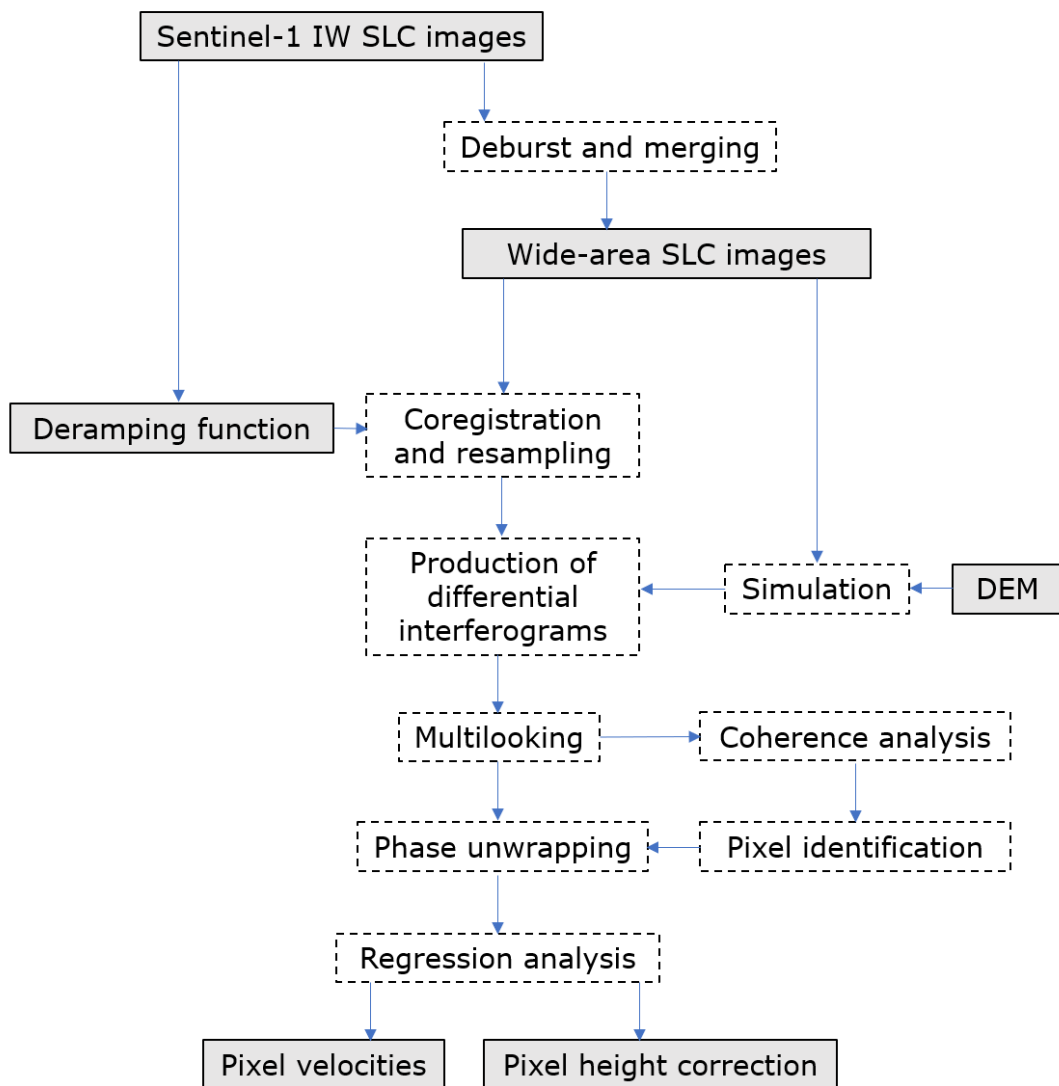
Figure 2: A flowchart summarising the steps undertaken for InSAR processing using the APSIS method to create a surface motion product from Sentinel-1 IW SLC imagery. Boxes shaded grey represent data sets, boxes with dotted borders represent processing steps. Modified from Sowter et al. (2016).

In order to interpret the resultant surface motion dataset produced by the ASPIS InSAR method, two sets of additional data were sourced: (i) higher resolution remote sensing data and (ii) meteorological data. The former

215 included orthophotos captured of the eight target areas by occupied airborne surveys commissioned by the
216 Swedis~~h~~ h Mapping, Cadastral and Land Registration Authority ~~Survey~~ (www.lantmateriet.se; © Lantmäteriet).
217 The ~~orthophotos~~ orthophotos (Lantmäteriet, 2021) have scenes ~~were panchromatic, with each scene~~ covering a
218 5km × 5km area, at a 0.5m spatial resolution, the majority were captured in 202~~16~~1, although gaps were filled
219 with imagery from 201~~0~~8 for two sites~~and 2008~~. The Swedish National Digital Elevation Model (DEM), was also
220 used in this study. The DEM was derived via occupied airborne LiDAR data capture between 2013~~in 2016~~ and
221 2018 (Table 1) processed to compute elevation at 2m spatial resolution across Sweden (www.lantmateriet.se; ©
222 Lantmäteriet). The orthophotos and DEM provided elevation and landscape characteristics (geomorphic features)
223 for use in this study. The meteorological data was captured by the Swedish Metrological and Hydrological Institute
224 (www.smhi.se) at meteorological stations across the region. Specifically, the air temperature, precipitation, and
225 snow depth data, were sourced and used from specific stations, i.e., those located closest to the palsa complexes
226 under investigation namely at ~~Katterjåkk,~~ Abisko, Kiruna, ~~and~~ Karesuando, Saarikoski, and ~~A~~Naimakka (Fig. 1).

227

2.3 Data analyses

229 2.3.1 Surface motion statistics

230 The ASPIS InSAR surface motion dataset was clipped to the 100m x 100m spatial resolution of the whole palsa
231 dataset and separately to the eight palsa complexes~~resampled using the mean value from the original 20m × 20m~~
232 ~~to match the 100m × 100m spatial resolution of the palsa peatland dataset which makes up the eight palsa~~
233 ~~complexes~~ (Backe, 2014). From this the frequency distributions of ASPIS InSAR surface motion at these eight
234 palsa complexes, and over all individual palsa peatland ~~pixels~~ raster cells in the region, were produced. Using
235 these data, the maximum and minimum rates of surface motion at each site was determined, as well as the sum of
236 the pixels with palsas that showed subsidence. These derived data relating to surface motion were further
237 interpreted using the orthophotos and DEMs, supported by the meteorological data.

238 2.3.2 Roughness thresholds

239 The DEM tiles were joined together and clipped to the eight palsa complexes. Following this, the degree of
240 elevation roughness was calculated, via the native topographic roughness index function (Riley, DeGloria, &
241 Elliot, 1999). This roughness index was thresholded at > 0.5 to provide a visual depiction of palsa landform edges
242 in the otherwise typically even terrain of the valley bottoms where the palsas occur. The roughness data was
243 visually compared to the orthophotos from a subset of areas to assess its potential for delineating palsas and this
244 allowed us to determine a threshold value that connected these continuous terrain variables to the specific features
245 of the palsa complexes, such as the raised mound structure of the palsa – so-called palsa mounds (Franklin, 2020).
246 Hillshade was also calculated via the native QGIS function using the default formula, which uses a lighting effect
247 to visualise the roughness of the terrain from differences in local elevation (QGIS, 2022). The roughness,
248 hillshade, and elevation outputs were overlaid on the mapped palsa tiles to provide higher resolution visual
249 interpretation.

250 2.3.3. Causes of surface motion

251 To test for the causes of surface motion palsa ASPIS InSAR surface motion was compared against roughness,
252 elevation and palsa percentage provided with the palsa raster cells (Backe, 2014). The roughness, ~~and~~ elevation
253 and InSAR outputs were ~~also~~ resampled to the resolution of the mapped palsa tiles (100m x 100m) to enable
254 statistical comparison. The zonal statistics tool was used to extract mean average values from the resulting
255 roughness and elevation outputs for the 100m spatial resolution mapped palsa tiles.

256 To analyse the relationships between surface motion, roughness and percent palsa in each 100m by 100m pixel
257 stratified by palsa complex, SciPy statistics (Virtanen et al., 2020) was used to obtain Pearson's correlation
258 statistics with an alpha value of 0.05 used to test for significance. Pandas (McKinney, 2011) and NumPy (Harris
259 et al., 2020) were used for data management. All scripts are available on the project GitHub
260 (https://github.com/SamValman/Permafrost_Sweden).

261 2.3.4 ~~C~~Climatic factors

262 Mean annual, maximum, and minimum daily air temperature, precipitation, and depth of ground snow for the
263 period 2000 to 2022 from the meteorological station nearest to a correspondent palsa complex were extracted and
264 analysed. The Naimakka station did not ~~provide~~ record snow depth and the Saarikoski station did not ~~provide~~
265 record air temperature, however, it was deemed that at the regional scale of this study these sites were sufficiently
266 close together (18km) to be ~~interchangable~~interchangeable. Subsequently, data was averaged to provide an annual
267 measurement of each meteorological variable for each station/palsa complex. Due to incomplete
268 ~~meterological~~meteorological datasets, a longer-term record of the meteorological variables was not possible for
269 all sites. However, long-term climate data (>100years) was available from three meteorological stations in the
270 region: namely, Karesuando, Kiruna, and Abisko. This data was used to assess temporal variability in annual,
271 winter (December, ~~January~~January, and February (DJF)) and summer (June, July, and August (JJA)) temperature,
272 precipitation and snowfall since the start of records across the region. Descriptive statistics (mean, minimum,
273 maximum and inter-quartile range) were produced to express the regional differences between these sites. Lastly,
274 to complement the point based meteorological (both weather and climate) data, we used modelled permafrost
275 probabilities based on climatic conditions to explore relationships between climatic conditions (Obu et al., 2018)
276 and subsidence rates ~~(Obu et al., 2018)~~. In this context, it is worth noting that there may be a mismatch between
277 the modelled permafrost distribution and permafrost in palsa areas ~~peatlands~~ as this can, in some areas, be a relic
278 of cooler climatic conditions. ~~The~~We used the mean values from the roughness and InSAR data to resample to
279 100m spatial resolution in line with the permafrost raster cells and spatially joined the permafrost probability
280 layer, taking the mean value where the 100m cell straddled multiple permafrost probability cells. ~~these data on~~
281 ~~permafrost probability were used to resampleto a 100m spatial resolution to enable comparison with the other data~~
282 ~~sets.~~

283 ~~To analyse the relationships between surface motion, roughness and percent palsa in each 100m by 100m pixel~~
284 ~~stratified by palsa complex, SciPy statistics (Virtanen et al., 2020) was used to obtain Pearson's correlation~~
285 ~~statistics. Pandas (McKinney, 2011) and NumPy (Harris et al., 2020) were used for data management. All scripts~~
286 ~~are available on the project GitHub (https://github.com/SamValman/Permafrost_Sweden).~~ The relationship
287 between the meteorological variables both over the last two decades at the weather stations closest to the palsa
288 complexes and duration of the climate record at the three weather stations with the longest data series were
289 assessed using linear regression analysis in Genstat (VNS Ldt). Assumptions of normality and homogeneity of
290 variance of the residuals were assessed using residual plots in Genstat. Some of time series were incomplete, in
291 these instances the analysis was conducted using the slightly shorter time series (see fig. 8).

292

293 **3.0 Results**

294 3.1 Surface motion

295 The ASPIS InSAR-derived surface motion outputs for the time-period of interest (2017-2021), ranged between
296 -9.9 and 7.7mm yr^{-1} across all of the palsa raster cells measured in northern Sweden, with a mean of 0.05, median
297 of 0.2 and range of 17.7mm yr^{-1}. Focusing solely on the eight palsa complexes provided greater insight and
298 excluded the most extreme uplift values from scattered individual palsas (Table 2). 69% of results were within
299 MSE of changing ground motion direction.

300

301

302

303

304 *Table. 2: InSAR subsidence and uplift measurements of the palsa complexes defined in Figure 1 and Table 1.*
305 *The total palsa area were used to isolate and extract ASPIS InSAR measurements of surface motion at each of*
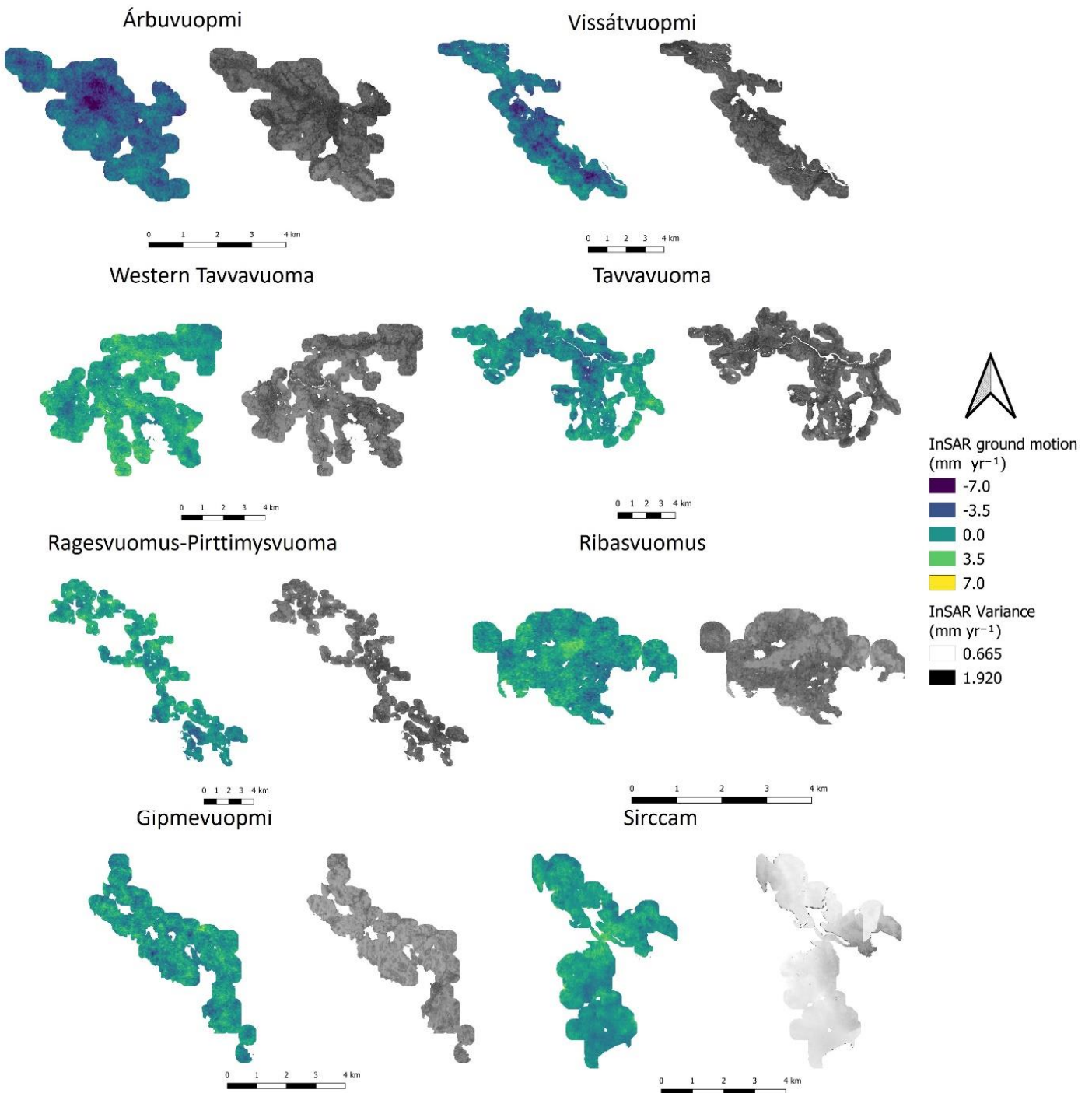306 *the eight sites.*

Site	Max subsidence	Max uplift (mm yr^{-1})	Subsiding area (ha)	Area subsiding >3.5 mm yr^{-1}	Mean standard error (mm yr^{-1})

	(mm yr^{-1})				(ha)
Árbuvuopmi	-9.9	1.7	321.3	138.4	<u>1.5</u>
Vissátvuopmi	-8.9	3.5	796.2	204.8	<u>1.5</u>
Tavvavuoma Western	-6.4	6.6	1009.4	50.9	<u>1.4</u>
Tavvavuoma	-5.1	6.3	215.0	1.0	<u>1.4</u>
Gipmevuopmi	-6.9	6.3	117.2	1.8	<u>1.2</u>
Ragesvuomus-Pirttimysvuoma	-5.9	5.7	358.6	7.4	<u>1.4</u>
Sirccam	-3.1	5.4	135.3	0.0	<u>0.9</u>
Ribasvuomus	-6.5	5.5	93.6	0.7	<u>1.3</u>

307

308

309 The spatial plots of surface motion for each palsa complex displayed in Figure 3, illustrates ~~patterns of~~a spatiality
310 ~~in terms of~~ surface motion (both subsidence and uplift and associated variance) across this northern Sweden
311 region. This is evident both within the palsa complexes and between the complexes.

Figure. 3: Palsa ground motion measured using Satellite InSAR from 2017 to 2021, showing differing levels of degradation across the eight study sites. Sites are ordered by their latitudinal position. Negative values correspond to subsidence. Note that in order to plot continuous areas the scenes shown are the palsa ~~peatland~~ area plus a 250m buffer around each 100m ×100m ~~pixel~~ raster cell that cover a minimum of 1% palsa (Backe

319   *2014). This means that areas of non-palsa peatland and some areas with mineral soil are included in the figure.*

320   *ASPIS InSAR variance were less than 1.5mm yr^{-1} in over 90% of pixels.*

321

322   ~~Subsidence was recorded in just under half of the pixels all the eight palsa complexes (Table 2).~~ Across the target

323   sites 3046.6ha (Table 2) out of the total site area of 5523ha (Table 1) were subsiding, which equates to ca 55% of

324   the total palsa complexes' area. Out of the subsiding parts of the palsa complexes, 405ha were subsiding at rates

325   >3.5mm yr^{-1} at near gaussian distribution. However, it is evident from the frequency distribution plots, that it is in

326   the palsa complexes in the far north of the region that subsidence dominated the surface motion measured (Table

327   2, Fig. 4). At Vissátvuompi and Árbuvuopmi 98 and 92% of the palsa complexes were subsiding with maximum

328   subsidence rates of -9.9 and -8.9mm yr^{-1}, respectively. The measured area affected by high subsidence rates of

329   between (>3.5mm yr^{-1}) were 204.8ha and 138.4ha at Vissátvuompi and Árbuvuopmi, respectively. This means

330   that ca. 30% of the total combined area of these two sites (1194ha) is in the highest range of subsidence. The high

331   degree of palsa subsidence at Vissátvuompi and Árbuvuopmi was confirmed by field observations at these sites

332   (Sofie Sjogersten, pers. Obs.): Both sites showed signs of active lateral erosions, large scale subsidence and

333   thermokarst formation. The more southerly sites also show subsidence, although ground motion rates were much

334   ~~lower~~more stable, with the -1 and 1mm yr^{-1} range being most common (Fig. 4). Areas further to the south and

335   west showed signs of uplift, particularly the western parts of Tavvavuoma and Ribasvuomus with maximum rates

336   of uplift of 6.3mm across some smaller parts of these sites. However, all sites have some degree of subsidence,

337   albeit at a lower rate compared to the heavily subsiding northern sites.

338
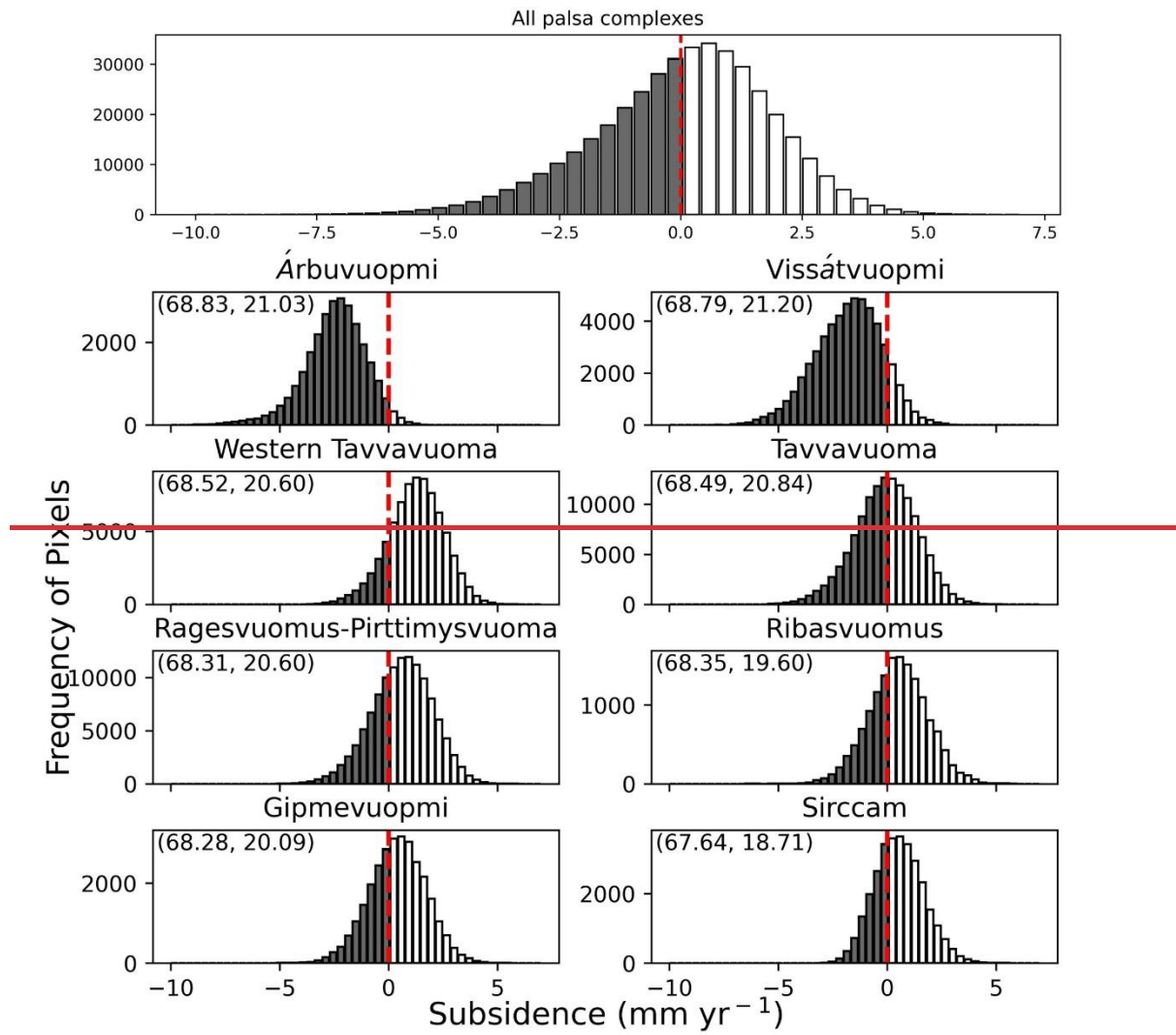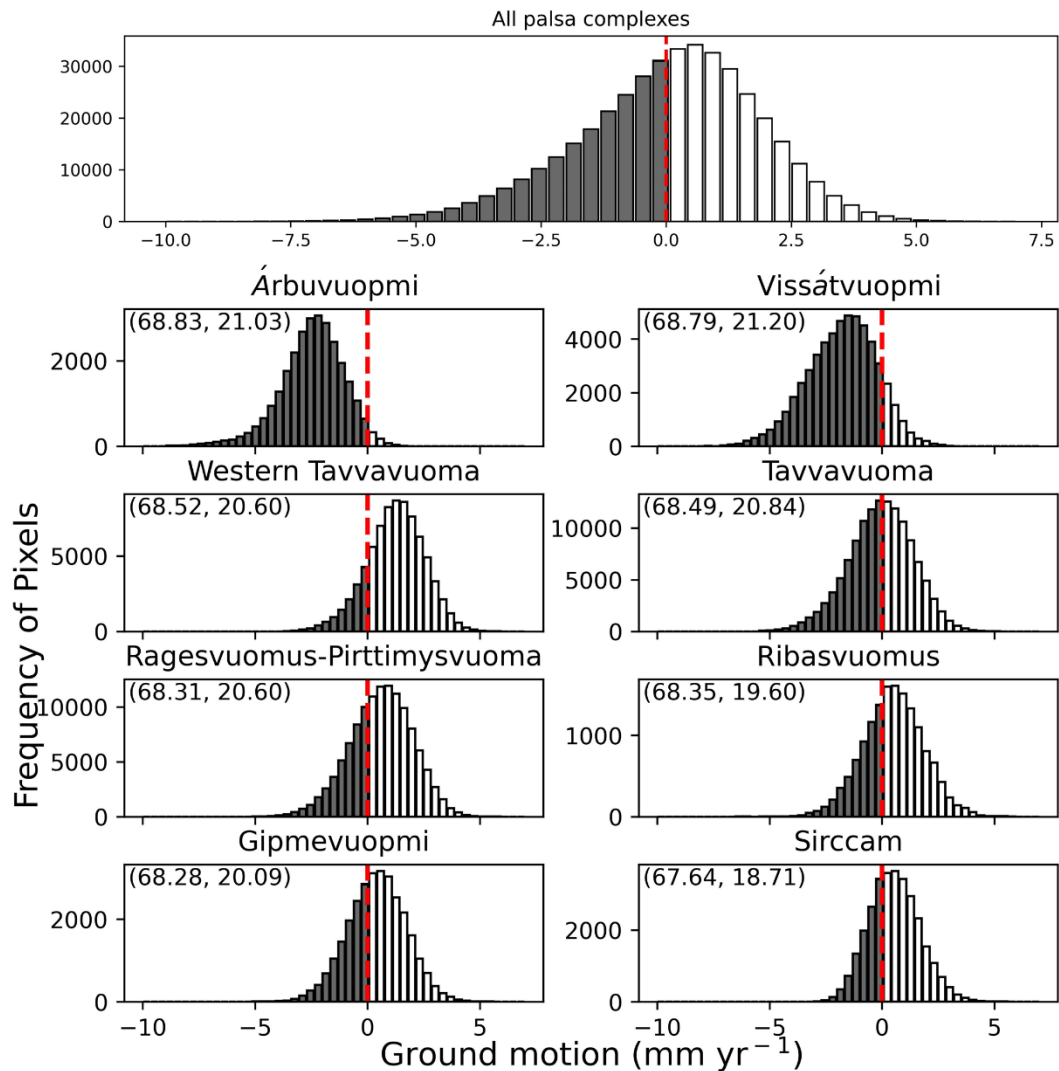
Figure. 4: Distribution of 20m ×20m ASPIS InSAR pixels within each of the palsa complexes in this study and the overall trend of the dataset according to the distribution of pixel moving in a particular direct and a given rate. Shaded areas with negative values correspond to subsidence. The dashed central lines indicate pixels in stable areas with no motion. Central point latitude and longitude is provided for each site in brackets for each site.

3.2 Topographic drivers and indicators

Calculating the roughness index from the DEMs at each palsa complex enabled differentiation of palsa from surrounding lower lying and flat fen areas. Representative example complexes are shown in Figures 5 and 6 - Vissátvuopmi and Western Tavvavuoma, Overall, the palsa complexes to the north (e.g., Fig. 5b, c) display a more pronounced topography across the focus areas than the more south-westerly ones (e.g., Fig. 6b, c). There was clear correspondence between density of palsa and subsidence, i.e., areas with more palsa showed more subsidence (Fig. 5a, d). Furthermore, the palsa complexes showed greater elevation variation compared to surrounding fen areas and were more densely clustered to the north than in the more south westerly sites. These features spatially coincided with higher subsidence. Substantial within site variability in subsidence was evident, where the pixels with the highest subsidence rates being clustered together and following landscapes features, e.g., palsa plateaux edges. It was evident that many separate palsa complexes in an area resulted in a high degree of elevation change, causing a high roughness index. In turn, areas with high roughness have the greatest subsidence (Fig. 5,6). Visual comparison between orthophotos and roughness showed that areas of high roughness corresponded well with areas of severe permafrost degradation (as indicated by lateral erosion and thermokarst formation).

14
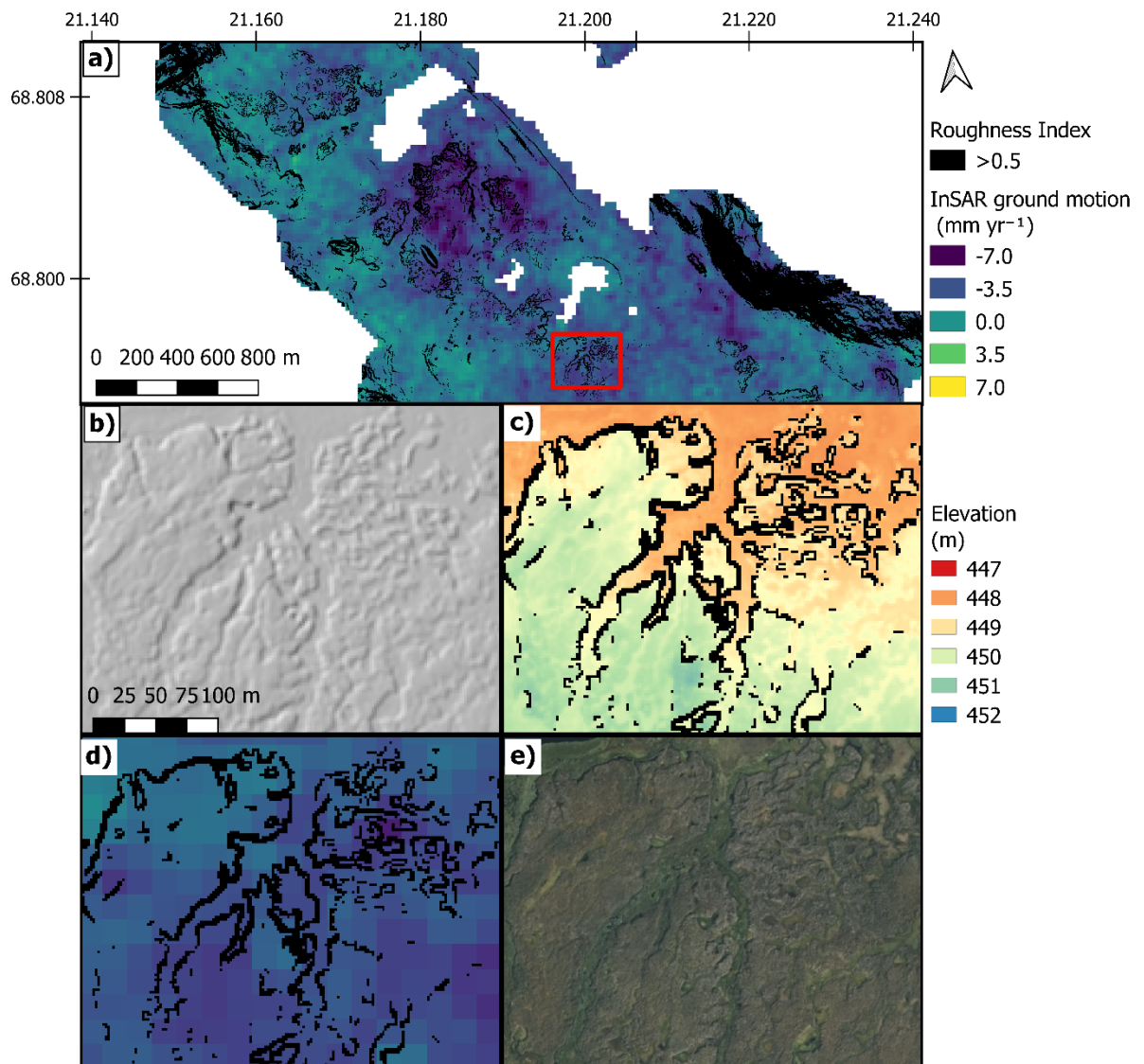
*Figure. 5: Visual analysis of Vissátvuopmi one of the sites where the most subsidence was found to be occurring. Evaluation of correspondence of hillshade DEM (b), DEM (c) and ~~a close look at~~ InSAR subsidence (d) with ~~Palsa~~ palsa complexes suggested by roughness overlays and aerial imagery (e). The positioning of b,c, and d within the larger site (a) show bands of subsidence ~~in~~ proximal to roughness patches suggesting ~~Palsa~~palsa.*
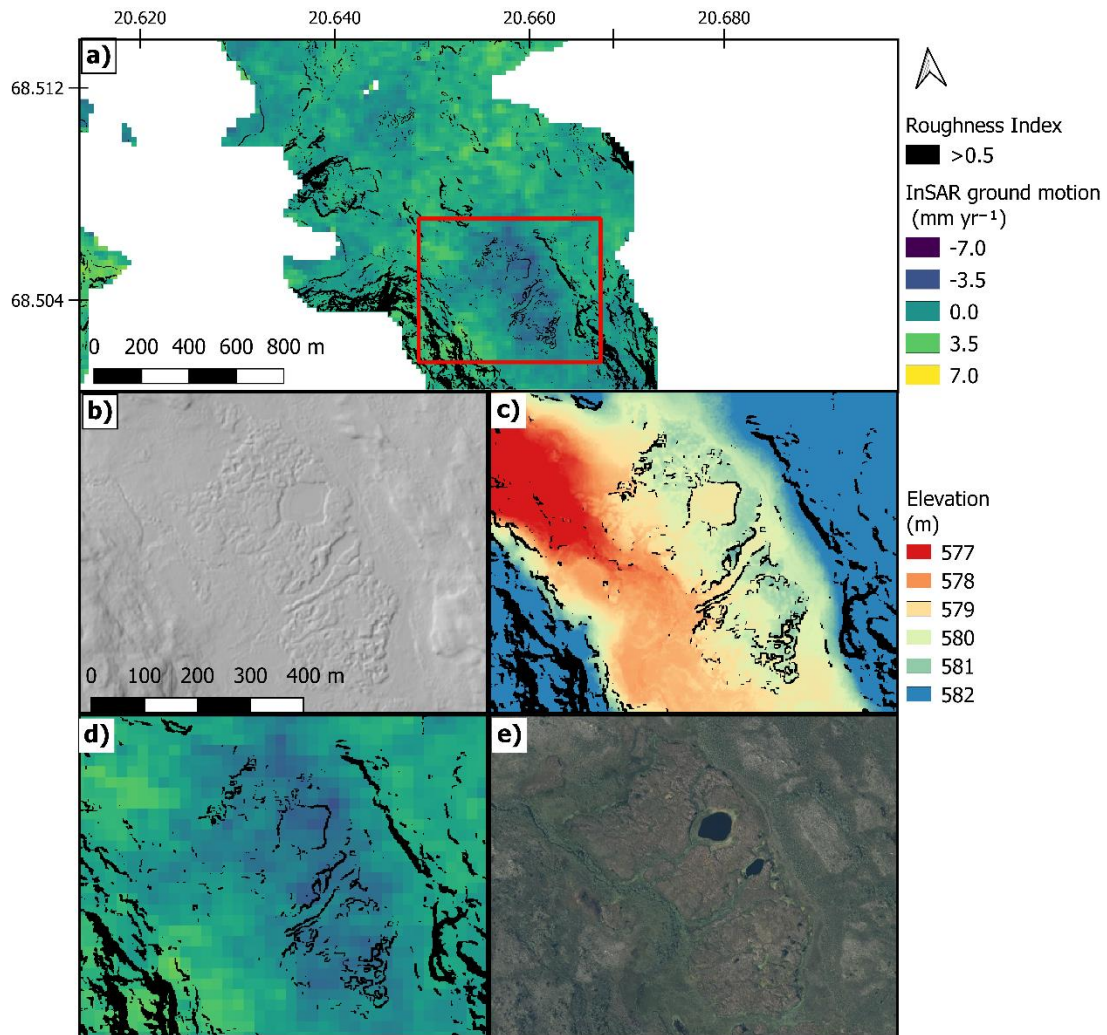
368

369 *Figure. 6: Visual analysis of Tavvavuoma which was found to have much lower levels of subsidence in*
370 *comparison to more northern sites. Evaluation of correspondence of hillshade DEM (b), DEM (c) and InSAR*
371 *subsidence (d) with Palsa complexes suggested by roughness overlays and aerial imagery (e). The positioning*
372 *of b,c, and d within the larger site (a) show many less "bands" (linear arrangements of palsa across the image)*
373 *of subsidence and potential palsa than Figure 4.*

374

375 Regression analysis showed a relationship between roughness and subsidence as sites with greater subsidence
376 were also found to have greater roughness (Fig. 7a). Higher percentage palsa in a location was linearly related to
377 subsidence with the greatest subsidence found in areas with the highest percentage palsa cover (Fig. 7b). It was
378 also clear that the modelled permafrost probability did not correspond to the percentage of palsa, i.e. pixels with
379 100% palsa are in some instances predicted to have no permafrost (Fig. 7b).

16

380

381
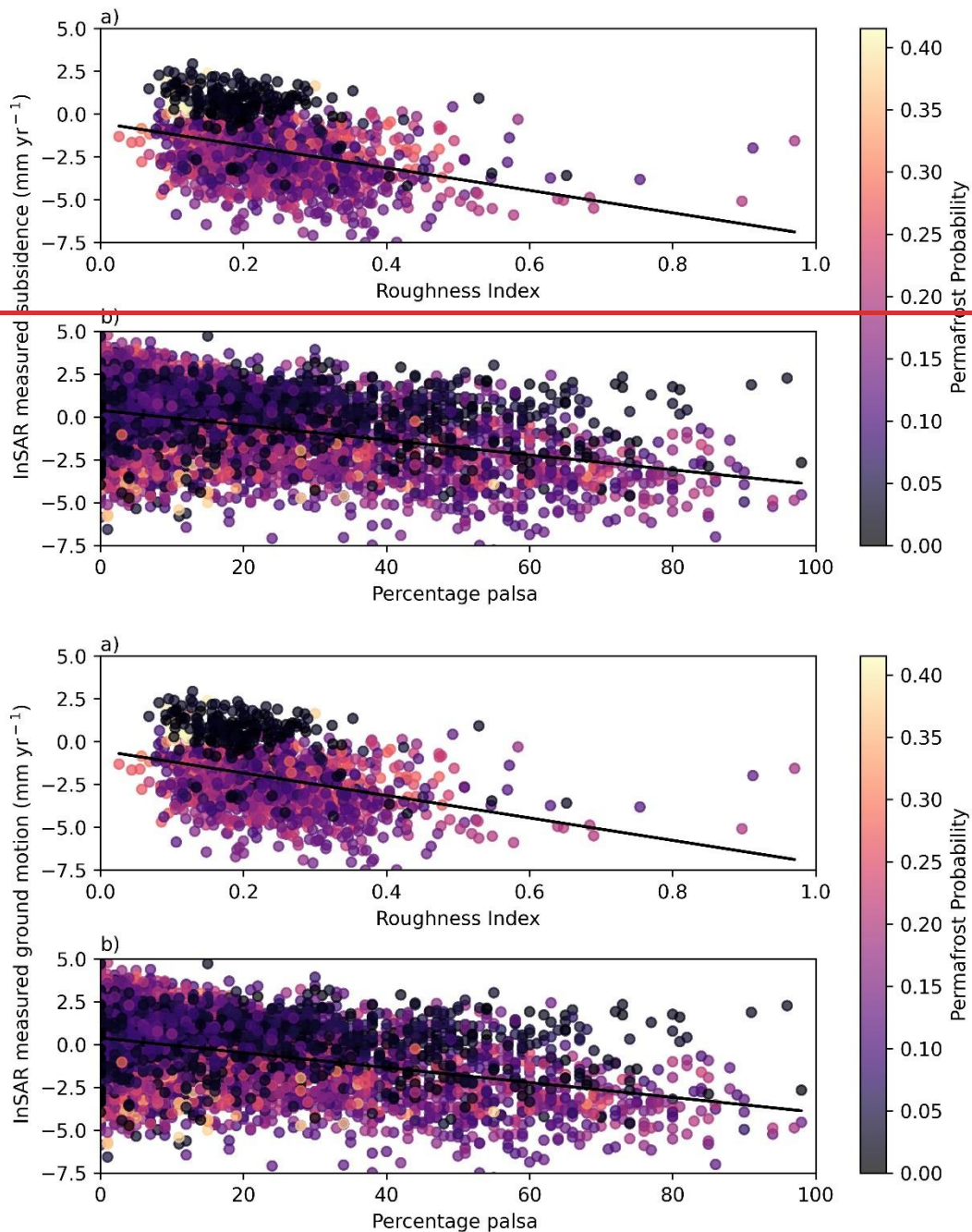
Figure. 7: Relationship between a) the roughness index; p < 0.001, R² = 0.35 and b) percentage palsa in a pixel; p < 0.001, R² = 0.41 and subsidence. The colours indicated for each data point are the analysed probability (on a scale from 0 to 1) that an area would include permafrost, (Obu et al., 2018). Note that there is less data for the analysis of roughness as the roughness was characterized only for the eight study sites and not all palsa ~~areas~~raster cells from (Backe, 2014). Roughness values from valley sides (which at time were included in the buffer areas) are not used in the figure.

382
383
384
385
386
387

3.4 Meteorological trends

388

The analysis of the ~~metrological~~meteorological data showed variability in both weather and climate across the study region in part reflecting the patterns in the subsidence data. The warmest minimum and maximum temperatures, -29.2 and 32.8°C respectively, were recorded for the palsa complexes north of Lake Tornetrask, i.e. Gipmevuomi and Ribasvuomus (Abisko weather station) (Fig. 1). The temperature in the area of Árbuvuopmi, Vissátvuopmi, and Tavvavuoma palsa complexes (Saarikoski/Naimaka and Karesuando weather stations) ranged between -39.4 and 30.5°C (Table 3, Fig. 8a). ~~The Katterjåkk weather station located in the mountains close to the~~

389
390
391
392
393
394

395 ~~Norwegian border recorded the greatest annual snow depth measure of 229cm and a mean of 50cm. Note that in~~
396 ~~this far western part of the study area palsa peatland were not present anymore. In contrast, t~~The ~~three other~~ sites
397 had comparable annual snow depth with a mean of 20-30cm (Table 3, Fig. 8b).

398

399
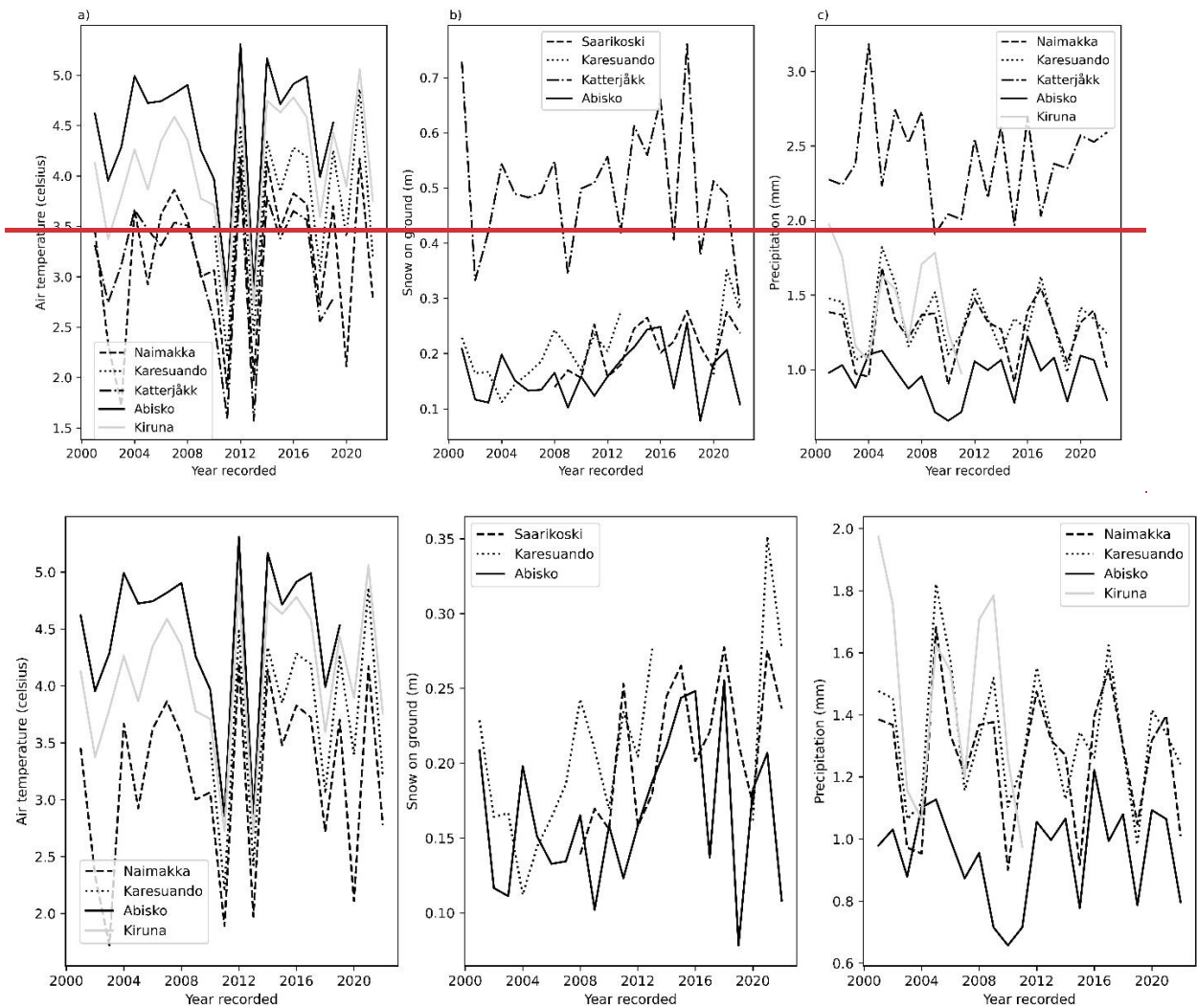
Figure. 8: ~~a)~~ Mean annual a) daily maximum temperature, b) snow depth on the ground, and c) daily
precipitation at the meteorological stations in the study region (SMHI 2022).

Table. 3: Temperature and snowfall descriptive statistics. The snow depth data are estimated from days with
snow on the ground. Mean annual temperature and precipitation are averaged from 2000 to 2021. Maximum,
minimum and the inter-quartile range are of daily maximum temperature and daily precipitation since 2000 are
also shown. Some weather stations lack certain years but were considered to have adequate coverage for this
task while two sites did not have sufficient data collection during the time period to be reliable and were shaded
out.

Weather Station	Temperature (°C)				Snow depth (m)			Precipitation (mm)		
	Mean annual	Max daily	Min daily	IQR daily	Mean annual	Max daily	IQR daily	Mean annual	Max daily	IQR daily
Naimakka	-1.40	29.5	-38.2	15.7				456	50.8	1.0
Saarikoski					76.9	0.85	0.43	422	43.6	0.9
Karesuando	-0.70	30.5	-39.4	16.9	75.1	1.00	0.40	490	53.2	1.1
~~Katterjåkk~~	~~-0.32~~	~~29.5~~	~~-27.6~~	~~13~~	~~183.0~~	~~2.29~~	~~0.97~~	~~875~~	~~104.3~~	~~3~~

18

| Abisko | 0.53 | 32.8 | -29.2 | 13.5 | 60.0 | 1.27 | 0.42 | 348 | 61.9 | 0.6 |
| Kiruna | 0.06 | 30.3 | -30.6 | 15.6 | 5.3 | 1.13 | 0.45 | 545 | 53.1 | 0.9 |

There was no detectable difference in climatic trends among the meteorological weather stations since 2001 for any of these sites (p > 0.05). In contrast, the longer-term climate records show a strong increase in winter precipitation over the last 140 years at Karesuando, the northern most weather station of the three with long term records available ($F_{1,136}$=122.33, p < 0.001; σ^2=47.0 %; Fig. 9a). This long-term trend was also evident, albeit less strong, in Kiruna ($F_{1,110}$ = 28.17, p < 0.001; σ^2=19.7 %; Fig. 9b). In Abisko, the pattern of increasing in winter (DJF) precipitation was less clear ($F_{1,108}$=8.29, p < 0.01; σ^2=6.3 %; Fig. 9c). Mean annual Snow depth, temperature, and summer precipitation (JJA) did not show clear temporal trends (data not shownSee supplementary materials).
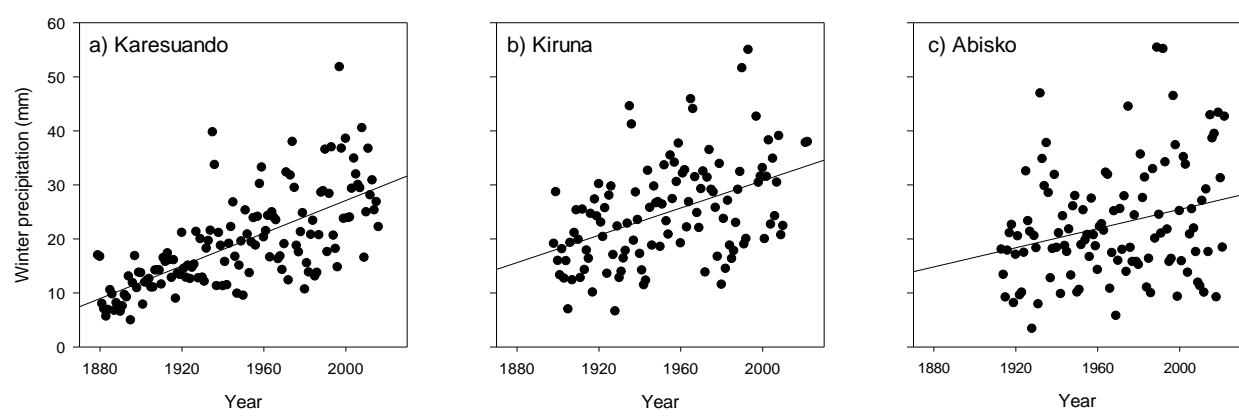
Figure 9. Mean winter (DJF) precipitation over time at a) Karesuando, b) Kiruna, and c) Abisko, significant trendlines are shown.

4. Discussion

By way of satellite ASPIS InSAR-derived surface motion and associated spatial and statistical analyses, we have demonstrated on-going, subsidence in the palsas peatlands of northern Sweden driven by a warming climate. Based on the compelling agreement of subsidence with palsa landforms and their roughness, we interpret this as permafrost degradation, i.e., thaw of the permafrost core within palsas and disintegration of these landforms. This is in line with a wide range of literature (see introduction) and concurs with the local-scale studies in the area undertaken using both satellite- and field-based methods (de la Barreda-Bautista et al., 2022; Olvmo et al., 2020; Sannel, 2020; Sannel et al., 2016; Sannel & Kuhry, 2011). The findings also agree with, as well as with, what is expected from the severe climate warming impacts on temperatures and precipitation noted in the region (Hänsel, 2020; Irannezhad et al., 2017; Vikhamar-Schuler et al., 2016) and the modelled predictions of total loss of permafrost across the region within decades (Fewster et al., 2022). We suggest that the surface subsidence of the sample palsa complexes measured in this study, together with complementary work in Norway (Borge et al., 2017), can be taken as evidence of significant substantial permafrost degradation in many all palsa peatland areas across northern Sweden and therefore, likely to be also occurring across northern Fennoscandia.

The processes driving the degradation of the permafrost, as measured by the ASPIS InSAR-derived subsidence data, are complex. Although permafrost degradation was observed in all the palsa complexes, rates varied both within and among palsa complexes (Table 2, Fig. 3 and 4). Overall, the InSAR subsidence data demonstrates a north south to south north gradient in increasing degradation. This indicates that local factors, such as local climate warming responses or permafrost temperature, determine the sensitivity of particular areas and that

446 regional climatic gradients play a role in the long-term trajectory of these ecosystems (Johansson et al., 2011;
447 Olvmo et al., 2020). In particular, winter precipitation is generally considered a strong predictor of permafrost
448 degradation due to the highly insulating properties of snow, preventing heat dissipation during winter (Olvmo et
449 al., 2020; Seppälä, 2011). This points to increased winter precipitation in the part of the northern most part of
450 study areas as a driver of the higher subsidence rates at the northern most palsa complexes (Table 2 and Fig. 8a).
451 Interestingly, climate data from the last two decades did not reveal strong differences in climatic conditions over
452 the area. This suggests that long-term trends combined with a buffered system reaction to change are driving
453 regional patterns in permafrost degradation.

454 It could also be the case that the observed north to south gradient of subsidence rates reflect different phases of
455 progression in an ongoing trend of permafrost degradation across the study region of northern Sweden. It is
456 plausible that the degradation process has progressed further at the more southern sites, reflecting higher
457 permafrost temperatures, and that as a result, subsidence rates have now slowed. All the while at the northern
458 sites, which still have a high cover of palsa: 26.3 and 31.6 % at Árbuvuopmi and Vissátvuopmi respectively,
459 show high subsidence rates. This is supported by research showing rapid permafrost degradation in the
460 southernmost palsa complexes in Sweden (Zuidhoff, 2002; Zuidhoff & Kolstrup, 2000) and in the area around
461 and to the south of Tornetrask, since the 1960's (Åkerman & Johansson, 2008; de la Barreda-Bautista et al.,
462 2022; Varner et al., 2022). However, permafrost degradation in palsas ~~peatlands~~ ha~~ve~~s progressed over longer-
463 time periods even in ~~the far~~ northern Fennoscandia ~~of Scandinavia~~. Here palsas' have decreased in areal extent
464 by 33– 71% over ca. 60 years, with more rapid contraction in recent years in Finmarkvidda, Norway and 54% in
465 Vissátvuopmi, northern most Sweden (Borge et al., 2017; Olvmo et al., 2020) and total loss of palsa complexes
466 has been recorded in the far north eastern parts of Norway (Vorren 2017).

467 Although there are differences in subsidence rates among sites the region wide permafrost degradation reflects
468 ongoing climatic trends (Fig. 3 and 7). Since 1901 Fennoscandia~~Scandinavia~~'s climate has become wetter as
469 well as warmer with a greater proportion of the precipitation falling as rain relatively to snow (Hänsel, 2020;
470 Irannezhad et al., 2018; Irannezhad et al., 2017; Vikhamar-Schuler et al., 2016). These trends are reflected in the
471 far north where higher air temperatures, greater precipitation and snow depths has already shifted climatic
472 conditions, in parts of the region, away from those that support permafrost in peatlands e.g. since the 1940's
473 (Åkerman & Johansson, 2008; Borge et al., 2017; Olvmo et al., 2020). Further, deep permafrost boreholes show
474 decadal signals of increasing temperatures in the Scandes mountains suggesting that warmer temperatures have
475 been impacting permafrost since the 1920's (Isaksen et al., 2007). Hence, is seems that climate warming has
476 been impacting permafrost in ~~Scandinavia~~ Fennoscandia for at least 100 years.

477 As a result of the ongoing trend of increasing permafrost temperatures in palsas ~~peatlands~~ in
478 ~~Scandinavia~~Fennoscandia, their permafrost temperatures are now close to 0°C, making them ~~very~~ especially
479 vulnerable to decay in response to further increases in temperatures (Christiansen et al., 2010; Farbrot et al.,
480 2013). Palsa formation is closely linked to the mean annual temperature, with temperatures ~~between~~ below -1 to
481 -2°C ~~over~~ and limited insulating snow cover over ~consecutive years needed as a threshold for palsas to form
482 (Vorren, 2017). In this context it is important to note that the MAT in the area was between 0.53 and -1.4^{o}C
483 since 2000 suggesting that at least in parts of the study area the climatic conditions do not support formation of
484 palsa anymore while conditions are marginal for palsa preservation in the entire region.

485 Although subsidence dominated in the northern sites, uplift was also noted in the study region. Mechanisms that
486 may explain patterns of uplift are formation of new palsa as well as short-lived frost mounds that can form
487 temporarily in the palsa system (Zuidhoff, 2002). Further mechanisms that may result in uplift are changes in
488 the water level of the flooded parts of the peatlands as well as accumulation of plant residues from the
489 productive fen vegetation parts of the study sites on the peatland surface, reflecting adaptation of the local
490 ecosystem to degraded palsa mounds reflected by changes in remotely sensed terrain surface.

491 In addition to demonstrating regional permafrost degradation in northern Fennoscandia, this work also provides
492 proof of concept for circumpolar assessments of permafrost degradation using ASPIS InSAR. It enables
493 detection of the areas with rapidly degrading permafrost and deepening active layers but also peat consolidation
494 in areas that ha~~ve~~s already lost its permafrost (de la Barreda-Bautista et al., 2022). The fact that InSAR data is
495 integrated over 20m × 20m pixels means that the signal of local level degradation may be somewhat dampened
496 (de la Barreda-Bautista et al., 2022). However, the high precision of the change in vertical position means that
497 InSAR is an important tool to employ to detect the initial stages of large-scale permafrost degradation.~ In
498 concurrence with the literature (Alshammari et al., 2020; Alshammari et al., 2018; Bartsch *et al.*, 2016; de la

Barreda-Bautista et al., 2022; Short et al., 2014; van Huissteden et al., 2021), we found the majority (69%) of our results were within the MSE of direction of ground motion change, providing confidence to locate where permafrost is degrading. Currently, the study of long-term trends and drivers using InSAR is somewhat limited by the short collection period of Sentinel 1, but as more data are continued to be collected, methods such as non-linear time series creation will become viable to compare subsidence directly to longer climatic drivers. However, the our large-scale baseline assessment of permafrost subsidence, provides a baseline to direct, and compare, against future fieldwork monitoring in northern Sweden developed here, provides an initial assessment of ongoing subsidence. would be advantageous should field monitoring be arranged in the future. As a complement to the ASPIS-InSAR data, the novel roughness thresholding method used here together with contextual data proved a powerful tool to map and monitor changes (Franklin, 2020; Konig et al., 2019; Otto et al., 2012). This approach could be developed using machine learning methods to model palsa dynamics to better automate the extraction of palsa landform positions (Konig et al., 2019; Luoto & Seppälä, 2002). If accomplished, the operating extent of this tool could be vastly increased using the Arctic 2m DEM dataset over area were its quality is high enough to allow high resolution mapping of the degrading edges of raised palsa plateauxaus (Morin, 2016); Karlson et al., 2021). In turn this could be used to remove the stable centre of palsa plateaux and exclusively compare palsa edges to the roughness index, where we would expect to find a stronger correlation than there exists with the current palsa raster cells (Fig. 7a). It has been suggested that small, fragmented, and irregularly shaped palsa are more susceptible to erosion (Borge et al., 2017; Mamet et al., 2017, Beer et al. in review). We have not gone as far as to estimate this here but the possible palsa edges inferred from the roughness index, could be built upon for this understanding. Casual analysis of figures 5, 6 and the orthophotos provided in the supplementary materials would support these expectations. Together the ASPIS-InSAR and the DEM derived roughness index metrics offer novel ways of large scale monitoring of permafrost degradation. This will help to quantify the rate of palsa ecosystem collapse and transition to a non-permafrost state.

We conclude that permafrost degradation of palsas peatlands is occurring across northern Sweden, with the greatest rates of degradation and largest areas impacted being Sweden's two largest permafrost peatland complexes in the far north. This raises serious concerns that these systems will lose their permafrost entirely in the coming decades especially as climatic conditions are approaching the limits of sustaining palsa peatlands (Fewster et al., 2022). The implications of this rapid loss of permafrost is ecosystem collapse and loss, as the permafrost core is fundamental to the existence of palsa peatlands. Future research should focus on the implications of this collapse on increased CH_4 emissions (Glagolev *et al.*, 2011; Turetsky *et al.*, 2020; Varner *et al.*, 2022), carbon loss (Hugelius *et al.*, 2020), and thus the potential for strong climate feedbacks (IPCC, 2021) as well as using longer-time InSAR data as this becomes available to investigate regional variations in climatic drivers of permafrost degradation. Further, our study demonstrates that InSAR together with terrain data can be applied over continuous natural surfaces at a regional-scale to monitor permafrost degradation in palsa peatlands, offering a tool for circumpolar monitoring of climate warming impact on these systems.

5. Acknowledgement

6. Author contributions

SV: Carried out the majority of the data analysis and made a significant contribution to data interpretation, writing and finalising the manuscript text. Both SV and MS can be considered to have contributed equally to this work.

MS: Contributed to the conception of the study, contributed DEM and orthophoto data, carried out fieldwork to assess permafrost degradation, contributed and advised on data analysis and interpretation, contributed to structuring, writing, and refining the text. Both MS and SV can be considered to have contributed equally to this work.

DB: Contributed to the conception of the study, advised on the data analysis, and made a significant contribution to finalising the text.

ML: Provided data analysis, support on the InSAR processing, data interpretation, and writing of the text.

DG: Carried out the initial InSAR data processing

BBB: Contributed to the conception of the study and refining the text.

AS: Contributed to the conception of the study and advised on the InSAR data processing

SS: Conceived and directed the study, contributed to data analysis, carried out fieldwork to assess permafrost degradation and made a significant contribution to formulating and finalising the text.

SS, DB, AS and MS secured the funding for the project.

Code Availability

All the python scripts used to carry out these analyses are available at the github repository: https://github.com/SamValman/Permafrost_Sweden.

Data Availability statement

The Sentinel-1 datasets are freely available and can be obtained by searching and downloading the Interferometric Wide (IW) swath mode products for orbit track numbers 168 ?? and ?? 66 through the Copernicus Open Access Hub (https://scihub. copernicus.eu/dhus/#/home). The processed interferometric data and deformation maps are commercially sensitive and may be made available on reasonable request by email addressed to the corresponding author. All other datasets produced during this project will be uploaded on zenodo and the DOI provided once the article has been accepted.

References

Åkerman, H. J., & Johansson, M. (2008). Thawing permafrost and thicker active layers in sub-arctic Sweden. *Permafrost and Periglacial Processes*, *19*(3), 279-292. https://doi.org/10.1002/ppp.626

Alshammari, L., Boyd, D. S., Sowter, A., Marshall, C., Andersen, R., Gilbert, P., Marsh, S., & Large, D. J. (2020). Use of Surface Motion Characteristics Determined by InSAR to Assess Peatland Condition [https://doi.org/10.1029/2018JG004953]. *Journal of Geophysical Research: Biogeosciences*, *125*(1), e2018JG004953. https://doi.org/https://doi.org/10.1029/2018JG004953

Alshammari, L., Large, D. J., Boyd, D. S., Sowter, A., Anderson, R., Andersen, R., & Marsh, S. (2018). Long-Term Peatland Condition Assessment via Surface Motion Monitoring Using the ISBAS DInSAR Technique over the Flow Country, Scotland. *Remote Sensing*, *10*(7). https://doi.org/10.3390/rs10071103

Armstrong McKay, D. I., Staal, A., Abrams, J. F., Winkelmann, R., Sakschewski, B., Loriani, S., Fetzer, I., Cornell, S. E., Rockström, J., & Lenton, T. M. (2022). Exceeding 1.5°C global warming could trigger multiple climate tipping points. *Science*, *377*(6611), eabn7950. https://doi.org/doi:10.1126/science.abn7950

Backe, S. (2014). *Kartering av Sveriges palsmyrar*. Länsstyrelsen.

Ballantyne C. K. (2018). *Periglacial geomorphology*. John Wiley & Sons.

Bartsch, A., Widhalm, B., Kuhry, P., Hugelius, G., Palmtag, J., Siewert, M.B., 2016. Can C-band synthetic aperture radar be used to estimate soil organic carbon storage in tundra? *Biogeosciences*, 13, 5453-5470.

Beer, J. M., Wang, Y., Way, R., Forget, A. & Colyn, V. 2023. Uncrewed aerial vehicle-based assessments of peatland permafrost vulnerability along the Labrador Sea coastline, northern Canada.

Biskaborn, B. K., Smith, S. L., Noetzli, J., Matthes, H., Vieira, G., Streletskiy, D. A., Schoeneich, P., Romanovsky, V. E., Lewkowicz, A. G., Abramov, A., Allard, M., Boike, J., Cable, W. L., Christiansen, H. H., Delaloye, R., Diekmann, B., Drozdov, D., Etzelmüller, B., Grosse, G., . . . Lantuit, H. (2019). Permafrost is warming at a global scale. *Nature Communications*, *10*(1), 264. https://doi.org/10.1038/s41467-018-08240-4

Borge, A. F., Westermann, S., Solheim, I., & Etzelmüller, B. (2017). Strong degradation of palsas and peat plateaus in northern Norway during the last 60 years. *The Cryosphere*, *11*(1), 1-16. https://doi.org/10.5194/tc-11-1-2017

Bradley, A. V., Andersen, R., Marshall, C., Sowter, A., & Large, D. J. (2022). Identification of typical ecohydrological behaviours using InSAR allows landscape-scale mapping of peatland condition. *Earth Surf. Dynam.*, *10*(2), 261-277. https://doi.org/10.5194/esurf-10-261-2022

Chadburn, S. E., Burke, E. J., Cox, P. M., Friedlingstein, P., Hugelius, G., & Westermann, S. (2017). An observation-based constraint on permafrost loss as a function of global warming. *Nature Climate Change*, *7*(5), 340-344. https://doi.org/10.1038/nclimate3262

Chen, C.W. and Zebker, H.A., 2001. Two-dimensional phase unwrapping with use of statistical models for cost functions in nonlinear optimization. JOSA A, 18(2), pp.338-351.

Christiansen, H. H., Etzelmüller, B., Isaksen, K., Juliussen, H., Farbrot, H., Humlum, O., Johansson, M., Ingeman-Nielsen, T., Kristensen, L., Hjort, J., Holmlund, P., Sannel, A. B. K., Sigsgaard, C., Åkerman, H. J., Foged, N., Blikra, L. H., Pernosky, M. A., & Ødegård, R. S. (2010). The thermal state of permafrost in the nordic area during the international polar year 2007–2009. *Permafrost and Periglacial Processes*, *21*(2), 156-181. https://doi.org/https://doi.org/10.1002/ppp.687

Cigna, F., & Sowter, A. (2017). The relationship between intermittent coherence and precision of ISBAS InSAR ground motion velocities: ERS-1/2 case studies in the UK. *Remote Sensing of Environment*, *202*, 177-198. https://doi.org/https://doi.org/10.1016/j.rse.2017.05.016

de la Barreda-Bautista, B., Boyd, D. S., Ledger, M., Siewert, M. B., Chandler, C., Bradley, A. V., Gee, D., Large, D. J., Olofsson, J., Sowter, A., & Sjögersten, S. (2022). Towards a Monitoring Approach for Understanding Permafrost Degradation and Linked Subsidence in Arctic Peatlands. *Remote Sensing*, *14*(3). https:// doi.org/10.3390/rs14030444

Douglas, T. A., Hiemstra, C. A., Anderson, J. E., Barbato, R. A., Bjella, K. L., Deeb, E. J., Gelvin, A. B., Nelsen, P. E., Newman, S. D., Saari, S. P., & Wagner, A. M. (2021). Recent degradation of interior Alaska permafrost mapped with ground surveys, geophysics, deep drilling, and repeat airborne lidar. *The Cryosphere*, *15*(8), 3555-3575. https://doi.org/10.5194/tc-15-3555-2021

Douglas, T. A., Jorgenson, M. T., Brown, D. R. N., Campbell, S. W., Hiemstra, C. A., Saari, S. P., Bjella, K., & Liljedahl, A. K. (2015). Degrading permafrost mapped with electrical resistivity tomography, airborne imagery and LiDAR, and seasonal thaw measurements. *GEOPHYSICS*, *81*(1), WA71-WA85. https://doi.org/10.1190/geo2015-0149.1

ESA (2015). Definition of the TOPS SLC deramping function for products generated by the S-1 IPF. *European Space Agency*. COPE-GSEG-EOPG-TN-14-0025, Issue 1, Revision 2, 22 April 2015.

Farbrot, H., Isaksen, K., Etzelmüller, B., & Gisnås, K. (2013). Ground Thermal Regime and Permafrost Distribution under a Changing Climate in Northern Norway. *Permafrost and Periglacial Processes*, *24*(1), 20-38. https://doi.org/https://doi.org/10.1002/ppp.1763

Fewster, R. E., Morris, P. J., Ivanovic, R. F., Swindles, G. T., Peregon, A. M., & Smith, C. J. (2022). Imminent loss of climate space for permafrost peatlands in Europe and Western Siberia. *Nature Climate Change*, *12*(4), 373-379. https://doi.org/10.1038/s41558-022-01296-7

Franklin, S. E. (2020). Interpretation and use of geomorphometry in remote sensing: a guide and review of integrated applications. *International Journal of Remote Sensing*, *41*(19), 7700-7733. https://doi.org/10.1080/01431161.2020.1792577

Fronzek, S., Luoto, M., & Carter, T. (2006). Potential effect of climate change on the distribution of palsa mires in subarctic Fennoscandia. *Climate Research*, *32*(1), 1-12. https://www.int-res.com/abstracts/cr/v32/n1/p1-12/

Gee, D., Bateson, L., Sowter, A., Grebby, S., Novellino, A., Cigna, F., Marsh, S., Banton, C., & Wyatt, L. (2017). Ground Motion in Areas of Abandoned Mining: Application of the Intermittent SBAS (ISBAS) to the Northumberland and Durham Coalfield, UK. *Geosciences*, *7*(3). https://doi.org/10.3390/geosciences7030085

Gisnås, K., Etzelmüller, B., Lussana, C., Hjort, J., Sannel, A. B. K., Isaksen, K., Westermann, S., Kuhry, P., Christiansen, H. H., Frampton, A., & Åkerman, J. (2017). Permafrost Map for Norway, Sweden and Finland. *Permafrost and Periglacial Processes*, *28*(2), 359-378. https://doi.org/https://doi.org/10.1002/ppp.1922

Glagolev, M., Kleptsova, I., Filippov, I., Maksyutov, S., & Machida, T. (2011). Regional methane emission from West Siberia mire landscapes. *Environmental Research Letters*, *6*(4), 045214.

Hänsel, S. (2020). Changes in the Characteristics of Dry and Wet Periods in Europe (1851–2015). *Atmosphere*, *11*(10), 1080. https://www.mdpi.com/2073-4433/11/10/1080

Harris, C. R., Millman, K. J., van der Walt, S. J., Gommers, R., Virtanen, P., Cournapeau, D., Wieser, E., Taylor, J., Berg, S., Smith, N. J., Kern, R., Picus, M., Hoyer, S., van Kerkwijk, M. H., Brett, M., Haldane, A., del Río, J. F., Wiebe, M., Peterson, P., . . . Oliphant, T. E. (2020). Array programming with NumPy. *Nature*, *585*(7825), 357-362. https://doi.org/10.1038/s41586-020-2649-2

Harris, L. I., Richardson, K., Bona, K. A., Davidson, S. J., Finkelstein, S. A., Garneau, M., McLaughlin, J., Nwaishi, F., Olefeldt, D., Packalen, M., Roulet, N. T., Southee, F. M., Strack, M., Webster, K. L., Wilkinson, S. L., & Ray, J. C. (2022). The essential carbon service provided by northern peatlands. *Frontiers in Ecology and the Environment*, *20*(4), 222-230. https://doi.org/https://doi.org/10.1002/fee.2437

Hugelius, G. A., Loisel, J. A., Chadburn, S. A., Jackson, R. A., Jones, M. A., MacDonald, G., Marushchak, M., Olefeldt, D. A., Packalen, M., Siewert, M. A.., Treat, C. A.-O., Turetsky, M., Voigt, C. A., & Yu, Z. A. (2020). Large stocks of peatland carbon and nitrogen are vulnerable to permafrost thaw. *Proceedings of the National Academy of Sciences*, 117(34), 20438-20446. https://doi.org/10.1073/pnas.1916387117.

IPCC. (2021). *The Physical Science Basis. Contribution of Working Group I to the Sixth Assessment Report of the Intergovernmental Panel on Climate Change*. Cambridge University Press.

Irannezhad, M., Moradkhani, H., & Kløve, B. (2018). Spatiotemporal Variability and Trends in Extreme Temperature Events in Finland over the Recent Decades: Influence of Northern Hemisphere Teleconnection Patterns. *Advances in Meteorology*, *2018*, 7169840. https://doi.org/10.1155/2018/7169840

Irannezhad, M., Ronkanen, A.-K., Kiani, S., Chen, D., & Kløve, B. (2017). Long-term variability and trends in annual snowfall/total precipitation ratio in Finland and the role of atmospheric circulation patterns. *Cold Regions Science and Technology*, *143*, 23-31. https://doi.org/https://doi.org/10.1016/j.coldregions.2017.08.008

Isaksen, K., Sollid, J. L., Holmlund, P., & Harris, C. (2007). Recent warming of mountain permafrost in Svalbard and Scandinavia. *Journal of Geophysical Research: Earth Surface*, *112*(F2). https://doi.org/https://doi.org/10.1029/2006JF000522

Johansson, M., Åkerman, J., Keuper, F., Christensen, T. R., Lantuit, H., & Callaghan, T. V. (2011). Past and Present Permafrost Temperatures in the Abisko Area: Redrilling of Boreholes. *AMBIO*, *40*(6), 558. https://doi.org/10.1007/s13280-011-0163-3

Johansson, M., Callaghan, T. V., Bosiö, J., Åkerman, H. J., Jackowicz-Korczynski, M., & Christensen, T. R. (2013). Rapid responses of permafrost and vegetation to experimentally increased snow cover in sub-arctic Sweden. *Environmental Research Letters*, *8*(3), 035025. https://doi.org/10.1088/1748-9326/8/3/035025

693 Karlson, M., bastviken, D. & reese, H. (2021). Error characteristics of pan-arctic digital elevation
694   models and elevation derivatives in northern sweden. *Remote Sensing,* 13**,** 4653.
695

696 Köchy, M., Hiederer, R., & Freibauer, A. (2015). Global distribution of soil organic carbon – Part 1: Masses and
697   frequency distributions of SOC stocks for the tropics, permafrost regions, wetlands, and the world.
698   *SOIL*, *1*(1), 351-365. https://doi.org/10.5194/soil-1-351-2015
699 König, S., Schultz, J. A., Schoch, A., Blöthe, J., Schrott, L., & Thonfeld, F. (2019). Mountain Permafrost
700   Distribution Modeling–A Geomorphometry-Remote Sensing Approach for the Hohe Tauern National
701   Park, Austria. *Dreiländertagung der DGPF, der OVG und der SGPF in Wien, Österreich–*
702   *Publikationen der DGPF*, 28.
703 Könönen, O. H., Karjalainen, O., Aalto, J., Luoto, M., & Hjort, J. (2022). Environmental spaces for palsas and
704   peat plateaus are disappearing at a circumpolar scale. *The Cryosphere Discuss.*, *2022*, 1-37.
705   https://doi.org/10.5194/tc-2022-135
706 Lantmäteriet. (2021). Orthophoto (Ortofoto) [Online]. Version 2.7. Available at:
707   https://www.lantmateriet.se/globalassets/geodata/geodataprodukter/flyg--och-
708   satellitbilder/e_pb_ortofoto.pdf. Accessed on 10th January 2024.
709 Liu, L., Zhang, T., & Wahr, J. (2010). InSAR measurements of surface deformation over permafrost on the
710   North Slope of Alaska. *Journal of Geophysical Research: Earth Surface*, *115*(F3).
711   https://doi.org/10.1029/2009JF001547
712 Luoto, M., & Seppälä, M. (2002). Modelling the distribution of palsas in Finnish Lapland with logistic
713   regression and GIS. *Permafrost and Periglacial Processes*, *13*(1), 17-28.
714 Luoto, M., & Seppälä, M. (2003). Thermokarst ponds as indicators of the former distribution of palsas in
715   Finnish Lapland. *Permafrost and Periglacial Processes*, *14*(1), 19-27. https://doi.org/10.1002/ppp.441
716 Mamet, S. D., Chun, K. P., Kershaw, G. G. L., Loranty, M. M., & Kershaw, G. P. (2017). Recent Increases in
717   Permafrost Thaw Rates and Areal Loss of Palsas in the Western Northwest Territories, Canada.
718   *Permafrost and Periglacial Processes*, *28*, 619-633. https://doi.org/   10.1002/ppp.1951
719 Markkula, I., Turunen, M., & Rasmus, S. (2019). A review of climate change impacts on the ecosystem services
720   in the Saami Homeland in Finland. *Science of The Total Environment*, *692*, 1070-1085.
721   https://doi.org/https://doi.org/10.1016/j.scitotenv.2019.07.272
722 Matthews, J. A., Dahl, S.-O., Berrisford, M. S., & Nesje, A. (1997). Cyclic Development and Thermokarstic
723   Degradation of Palsas in the Mid-Alpine Zone at Leirpullan, Dovrefjell, Southern Norway. *Permafrost*
724   *and Periglacial Processes*, *8*(1), 107-122. https://doi.org/https://doi.org/10.1002/(SICI)1099-
725   1530(199701)8:1<107::AID-PPP237>3.0.CO;2-Z
726 McKinney, W. (2011). pandas: a Foundational Python Library for Data Analysis and Statistics.
727 Miglovets, M., Zagirova, S., Goncharova, N., & Mikhailov, O. (2021). Methane Emission from Palsa Mires in
728   Northeastern European Russia. *Russian Meteorology and Hydrology*, *46*(1), 52-59.
729   https://doi.org/10.3103/S1068373921010076
730 Morin, P., Porter, C., Cloutier, M., Howat, I., Noh, M.J., Willis, M., Bates, B., Willamson, C. and Peterman, K.
731   (2016). ArcticDEM; a publically available, high resolution elevation model of the Arctic. EGU General
732   Assembly 2016, Vienna, Austria.
733 Obu, J. (2021). How Much of the Earth's Surface is Underlain by Permafrost? *Journal of Geophysical Research:*
734   *Earth Surface*, *126*(5), e2021JF006123. https://doi.org/https://doi.org/10.1029/2021JF006123
735 Obu, J., Westermann, S., Kääb, A., & Bartsch, A. (2018). *Ground Temperature Map, 2000-2016, Northern*
736   *Hemisphere Permafrost* PANGAEA. https://doi.org/10.1594/PANGAEA.888600
737 Olvmo, M., Holmer, B., Thorsson, S., Reese, H., & Lindberg, F. (2020). Sub-arctic palsa degradation and the
738   role of climatic drivers in the largest coherent palsa mire complex in Sweden (Vissátvuopmi), 1955–
739   2016. *Scientific Reports*, *10*(1), 8937. https://doi.org/10.1038/s41598-020-65719-1
740 Otto, J. c., Keuschnig, M., Götz, J., Marbach, M., & Schrott, L. (2012). Detection of mountain permafrost by
741   combining high resolution surface and subsurface information–an example from the Glatzbach
742   catchment, Austrian Alps. *Geografiska Annaler: Series A, Physical Geography*, *94*(1), 43-57.
743   https://doi.org/10.1111/j.1468-0459.2012.00455.x
744 QGIS, D. (2022). QGIS User Guide: 24.2.1 Raster Analysis. Retrieved from
745   https://docs.qgis.org/3.16/en/docs/user_manual/processing_algs/gdal/rasteranalysis.html#hillshade
746 Ramage, J., Jungsberg, L., Wang, S. N., Westermann, S., Lantuit, H., & Heleniak, T. (2021). Population living
747   on permafrost in the Arctic. *Population and Environment*, *43*(1), 22-38.
748   https://doi.org/10.1007/s11111-020-00370-6
749 Reinosch, E., Buckel, J., Dong, J., Gerke, M., Baade, J., & Riedel, B. (2020). InSAR time series analysis of
750   seasonal surface displacement dynamics on the Tibetan Plateau. *The Cryosphere*, *14*(5), 1633-1650.
751   https://doi.org/10.5194/tc-14-1633-2020

752 Sannel, A. B. K. (2020). Ground temperature and snow depth variability within a subarctic peat plateau
753   landscape. *Permafrost and Periglacial Processes*, *31*(2), 255-263. https://doi.org/10.1002/ppp.2045
754 Sannel, A. B. K., Hugelius, G., Jansson, P., & Kuhry, P. (2016). Permafrost Warming in a Subarctic Peatland –
755   Which Meteorological Controls are Most Important?. *Permafrost and Periglacial Processes*, *27*(2),
756   177-188. https://doi.org/10.1002/ppp.1862
757 Sannel, A. B. K., & Kuhry, P. (2011). Warming-induced destabilization of peat plateau/thermokarst lake
758   complexes. *Journal of Geophysical Research: Biogeosciences*, *116*(G3).
759   https://doi.org/10.1029/2010JG001635
760 Schuur, E. A. G., McGuire, A. D., Schädel, C., Grosse, G., Harden, J. W., Hayes, D. J., Hugelius, G., Koven, C.
761   D., Kuhry, P., Lawrence, D. M., Natali, S. M., Olefeldt, D., Romanovsky, V. E., Schaefer, K.,
762   Turetsky, M. R., Treat, C. C., & Vonk, J. E. (2015). Climate change and the permafrost carbon
763   feedback. *Nature*, *520*(7546), 171-179. https://doi.org/10.1038/nature14338
764 Schuur, E. A. G., Vogel, J. G., Crummer, K. G., Lee, H., Sickman, J. O., & Osterkamp, T. E. (2009). The effect
765   of permafrost thaw on old carbon release and net carbon exchange from tundra. *Nature*, *459*(7246),
766   556-559. https://doi.org/10.1038/nature08031
767 Seppälä, M. (2011). Synthesis of studies of palsa formation underlining the importance of local environmental
768   and physical characteristics. *Quaternary Research*, *75*(2), 366-370.
769   https://doi.org/10.1016/j.yqres.2010.09.007
770 Siewert, M.B., 2018. High-resolution digital mapping of soil organic carbon in permafrost terrain using machine
771   learning: a case study in a sub-Arctic peatland environment. *Biogeosciences,* 15, 1663-1682.
772 Sjöberg, Y., Siewert, M.B., Rudy, A.C.A., Paquette, M., Bouchard, F., Malenfant-Lepage, J., Fritz, M., 2020.
773   Hot trends and impact in permafrost science. *Permafrost and Periglacial Processes*, 31, 461-471.
774 Short, N., LeBlanc, A.-M., Sladen, W., Oldenborger, G., Mathon-Dufour, V., & Brisco, B. (2014).
775   RADARSAT-2 D-InSAR for ground displacement in permafrost terrain, validation from Iqaluit
776   Airport, Baffin Island, Canada. *Remote Sensing of Environment*, *141*, 40-51.
777   https://doi.org/https://doi.org/10.1016/j.rse.2013.10.016
778 SMHI, (2022). Download Meteorological observations. Retrieved from
779   https://www.smhi.se/data/meteorologi/ladda-ner-meteorologiska-
780   observationer#param=airtemperatureInstant,stations=core,stationid=191910
781 Smith, M. W., & Riseborough, D. W. (1996). Permafrost monitoring and detection of climate change.
782   *Permafrost and Periglacial Processes*, *7*(4), 301-309.
783   https://doi.org/https://doi.org/10.1002/(SICI)1099-1530(199610)7:4<301::AID-PPP231>3.0.CO;2-R
784 Smith, S.L, O'Neill, H.B., Isaksen, K., Noetzli, J. and Romanovsky, V.E. (2022). The changing thermal state of
785   permafrost. *Nature Reviews Earth and Environment,* 3, 10-23.
786 Sowter, A., Bin Che Amat, M., Cigna, F., Marsh, S., Athab, A., & Alshammari, L. (2016). Mexico City land
787   subsidence in 2014–2015 with Sentinel-1 IW TOPS: Results using the Intermittent SBAS (ISBAS)
788   technique. *International Journal of Applied Earth Observation and Geoinformation*, *52*, 230-242.
789   https://doi.org/https://doi.org/10.1016/j.jag.2016.06.015
790 Spyder Website Contributors. (2021). Spyder IDE. Retrieved from https://www.spyder-ide.org/
791 Swingedouw, D., Ifejika Speranza, C., Bartsch, A., Durand, G., Jamet, C., Beaugrand, G., & Conversi, A.
792   (2020). Early Warning from Space for a Few Key Tipping Points in Physical, Biological, and Social-
793   Ecological Systems. *Surveys in Geophysics*, *41*(6), 1237-1284. https://doi.org/10.1007/s10712-020-
794   09604-6
795 Tarnocai, C., Canadell, J. G., Schuur, E. A. G., Kuhry, P., Mazhitova, G., & Zimov, S. (2009). Soil organic
796   carbon pools in the northern circumpolar permafrost region. *Global Biogeochemical Cycles*, *23*(2).
797   https://doi.org/https://doi.org/10.1029/2008GB003327
798 Torres, R., Snoeij, P., Geudtner, D., Bibby, D., Davidson, M., Attema, E., Potin, P., Rommen, B., Floury, N.,
799   Brown, M., Traver, I. N., Deghaye, P., Duesmann, B., Rosich, B., Miranda, N., Bruno, C., L'Abbate,
800   M., Croci, R., Pietropaolo, A., . . . Rostan, F. (2012). GMES Sentinel-1 mission. *Remote Sensing of
801   Environment*, *120*, 9-24. https://doi.org/https://doi.org/10.1016/j.rse.2011.05.028
802 Turetsky, M. R., Abbott, B. W., Jones, M. C., Anthony, K. W., Olefeldt, D., Schuur, E. A. G., Grosse, G.,
803   Kuhry, P., Hugelius, G., Koven, C., Lawrence, D. M., Gibson, C., Sannel, A. B. K., & McGuire, A. D.
804   (2020). Carbon release through abrupt permafrost thaw. *Nature Geoscience*, *13*(2), 138-143.
805   https://doi.org/10.1038/s41561-019-0526-0
806 Vallée, S., & Payette, S. (2007). Collapse of permafrost mounds along a subarctic river over the last 100 years
807   (northern Québec). *Geomorphology*, *90*, 162-170. https://doi.org/10.1016/j.geomorph.2007.01.019
808 van Huissteden, J., Teshebaeva, K., Cheung, Y., Magnússon, R. Í., Noorbergen, H., Karsanaev, S. V., Maximov,
809   T. C., & Dolman, A. J. (2021). Geomorphology and InSAR-Tracked Surface Displacements in an Ice-
810   Rich Yedoma Landscape. *Frontiers in Earth Science*, *9*(724).
811   https://doi.org/10.3389/feart.2021.680565

812 Varner, R. K., Crill, P. M., Frolking, S., McCalley, C. K., Burke, S. A., Chanton, J. P., Holmes, M. E., null, n.,
813   Saleska, S., & Palace, M. W. (2022). Permafrost thaw driven changes in hydrology and vegetation
814   cover increase trace gas emissions and climate forcing in Stordalen Mire from 1970 to 2014.
815   *Philosophical Transactions of the Royal Society A: Mathematical, Physical and Engineering Sciences*,
816   *380*(2215), 20210022. https://doi.org/10.1098/rsta.2021.0022
817 Vikhamar-Schuler, D., Isaksen, K., Haugen, J. E., Tømmervik, H., Luks, B., Schuler, T. V., & Bjerke, J. W.
818   (2016). Changes in Winter Warming Events in the Nordic Arctic Region. *Journal of Climate*, *29*(17),
819   6223-6244. https://doi.org/10.1175/JCLI-D-15-0763.1
820 Virtanen, P., Gommers, R., Oliphant, T. E., Haberland, M., Reddy, T., Cournapeau, D., Burovski, E., Peterson,
821   P., Weckesser, W., & Bright, J. (2020). SciPy 1.0: fundamental algorithms for scientific computing in
822   Python. *Nature methods*, *17*(3), 261-272.
823 Vorren, K.-D. (2017). The first permafrost cycle in Færdesmyra, eastern Finnmark, Norway? *Norsk Geografisk*
824   *Tidsskrift - Norwegian Journal of Geography*, *71*(2), 114-121.
825   https://doi.org/10.1080/00291951.2017.1316309
826 Zuidhoff, F. S. (2002). Recent decay of a single palsa in relation to weather conditions between 1996 and 2000
827   in Laivadalen, northern Sweden. *Geografiska Annaler Series A-Physical Geography*, *84A*(2), 103-111.
828   https://doi.org/10.1111/j.0435-3676.2002.00164.x
829 Zuidhoff, F. S., & Kolstrup, E. (2000). Changes in palsa distribution in relation to climate change in Laivadalen,
830   northern Sweden, especially 1960–1997. *Permafrost and Periglacial Processes*, *11*(1), 55-69.
831   https://doi.org/https://doi.org/10.1002/(SICI)1099-1530(200001/03)11:1